Monthly Notices
of the
ROYAL ASTRONOMICAL SOCIETY

Mon. Not. R. Astron. Soc. **412,** 748–764 (2011) doi:10.1111/j.1365-2966.2010.17940.x

Towards a complete treatment of the cosmological recombination problem

J. Chluba[1,2]★ and R. M. Thomas[1]★

[1]*Canadian Institute for Theoretical Astrophysics, 60 St George Street, Toronto ON M5S 3H8, Canada*
[2]*Max-Planck-Institut für Astrophysik, Karl-Schwarzschild-Str. 1, D-85740 Garching, Germany*

Accepted 2010 October 27. Received 2010 October 26; in original form 2010 October 18

ABSTRACT

A new approach to the cosmological recombination problem is presented, which completes our previous analysis on the effects of two-photon processes during the epoch of cosmological hydrogen recombination, accounting for *n*s–1s and *n*d–1s Raman events and two-photon transitions from levels with $n \geq 2$. The recombination problem for hydrogen is described using an *effective* 400-shell multilevel approach to which we subsequently add *all* important recombination corrections discussed in the literature thus far. We explicitly solve the radiative transfer equation of the Lyman-series photon field to obtain the required modifications to the rate equations of the resolved levels. In agreement with earlier computations, we find that 2s–1s Raman scattering leads to a delay in recombination by $\Delta N_{\rm e}/N_{\rm e} \sim 0.9$ per cent at $z \sim 920$. Two-photon decay and the Raman scattering from higher levels ($n > 3$) result in small additional modifications, and precise results can be obtained when including their effect for the first three to five shells. This work is a major step towards a new cosmological recombination code (COSMOREC) that supersedes the physical model included in RECFAST, and which, owing to its short run time, can be used in the analysis of future cosmic microwave background data from the *PLANCK Surveyor*.

Key words: cosmic background radiation – cosmological parameters – cosmology: observations – cosmology: theory.

1 INTRODUCTION

The *PLANCK Surveyor*[1] is currently observing the temperature and polarization anisotropies of the cosmic microwave background (CMB), and scientists all over the world eagerly await its first data release scheduled for early 2011. With *PLANCK* data sets, cosmologists will be able to determine key cosmological parameters with unprecedented precision, making it possible to distinguish between the various models of *inflation* (e.g. see Komatsu et al. 2010, for recent constraints).

Over the past five years, various groups (e.g. see Dubrovich & Grachev 2005; Chluba & Sunyaev 2006b; Kholupenko & Ivanchik 2006; Wong & Scott 2007; Chluba & Sunyaev 2008; Hirata 2008; Karshenboim & Ivanov 2008; Rubiño-Martín, Chluba & Sunyaev 2008; Switzer & Hirata 2008; Jentschura 2009; Labzowsky, Solovyev & Plunien 2009; Ali-Haïmoud & Hirata 2010; Grin & Hirata 2010) have realized that the uncertainties in the theoretical treatment of the cosmological recombination process could have important consequences for the analysis of the CMB data from the *PLANCK Surveyor*. It was shown that, in particular, our ability to measure the precise value of the spectral index of scalar perturbations, $n_{\rm S}$, and the baryon content of our Universe will be compromised if modifications to the recombination model by RECFAST (Seager, Sasselov & Scott 1999, 2000) are neglected (Rubiño-Martín et al. 2010).

To ensure that uncertainties in the cosmological recombination model do not undermine the science return of the *PLANCK* satellite, it is crucial to incorporate all important processes leading to changes in the free electron fraction close to the maxima of the Thomson visibility function (Sunyaev & Zeldovich 1970) by more than ∼0.1 per cent into *one* recombination module. The main obstacle towards accomplishing this so far was that detailed recombination calculations took too long to allow accounting for the full cosmological dependence of the recombination corrections on a model-by-model basis. This led to the introduction of *improved fudge factors* to RECFAST (Wong & Scott 2007; Wong, Moss & Scott 2008), or *multidimensional interpolation schemes* (Fendt et al. 2009; Rubiño-Martín et al. 2010), that allow fast but approximate representation of the full recombination code.

Although it was already argued that for the stringent error bars of today's cosmological parameters such approaches should be sufficient (Rubiño-Martín et al. 2010), from a physical stand point it would be much more satisfying to have a full representation of the recombination problem, that does not suffer from the limitations mentioned above, while capturing all the important physical processes simultaneously. Furthermore, such a recombination module increases the flexibility, and allows us to provide extensions, e.g. to account for the effect of *dark matter annihilation*, energy injection

★E-mail: jchluba@cita.utoronto.ca (JC); thomas@cita.utoronto.ca (RMT)
[1] www.rssd.esa.int/Planck.

by *decaying particles* (e.g. see Chen & Kamionkowski 2004; Padmanabhan & Finkbeiner 2005; Chluba 2010), or the *variation of fundamental constants* (Kaplinghat, Scherrer & Turner 1999; Galli et al. 2009; Scóccola, Landau & Vucetich 2009), while treating all processes simultaneously.

In this paper, we describe our new approach to the recombination problem, which enables us to fulfill this ambition by overcoming the problems mentioned above. Our code, called COSMOREC,[2] runs in 1–2 min for a given set of cosmological parameters as it stands and can be optimized further to run well below a minute, eliminating the need for *fudge factors* to solve the recombination problem. One of the key ingredients that facilitates this increase in speed is the effective multilevel approach which was proposed recently by Ali-Haïmoud & Hirata (2010).

We also extend our previous analysis on the effects of two-photon processes during the cosmological recombination epoch of hydrogen (Chluba & Sunyaev 2008, 2010b) to account for *n*s–1s and *n*d–1s Raman scattering and two-photon transitions from levels with $n \geq 2$. The radiative transfer equation for the Lyman-series photons during hydrogen recombination is solved in detail using a partial differential equation (PDE) solver that we developed for this purpose and can accommodate non-uniform grids (see Appendix B for more details). Our results for the effect of the Raman scattering on the recombination dynamics are in good agreement with earlier computations (Hirata 2008). Furthermore, we show that two-photon decays from levels with $n \gtrsim 4$–5 can be neglected and Raman scattering is only important for the first few shells.

The main difficulty with two-photon and Raman processes during the recombination epoch is the presence of resonances in the interaction cross-sections related to normal '1+1'-photon transitions that are already included into the multilevel recombination code (Chluba & Sunyaev 2008; Hirata 2008; Hirata & Switzer 2008; Chluba & Sunyaev 2010b). Unlike for the 2s–1s two-photon decay, all the higher *n*s–1s and *n*d–1s two-photon channels include '1 + 1'-photon sequences via energetically *lower* Lyman-series resonances, i.e. $n\mathrm{s/d} \leftrightarrow k\mathrm{p} \leftrightarrow 1\mathrm{s}$ with $k < n$. Similarly, for *n*s–1s and *n*d–1s Raman-scattering events, *all higher* Lyman-series resonances, i.e. $n\mathrm{s/d} \leftrightarrow k\mathrm{p} \leftrightarrow 1\mathrm{s}$ with $k > n$, appear. Therefore, special care has to be taken to avoid *double counting* of these resonances in the rate equations of the multilevel atom as we explain in Sections 3.4.3, 3.4.4, 3.5.3 and 3.5.4.

In Section 2, we outline our principal approach to the recombination problem. The terms for the radiative transfer equation that allow to take all important recombination corrections into account are derived in Section 3. We then solve the evolution equation for the high-frequency photon field during the recombination epoch, and illustrate the different changes in Section 4. In Section 5, we discuss the different corrections to the ionization history, and present our conclusions and outlook in Section 6.

2 PERTURBATIVE APPROACH TO SOLVING THE FULL RECOMBINATION PROBLEM

2.1 General aspects of the standard recombination problem

The cosmological recombination problem consists of determining an accurate estimate of the free electron fraction, $X_\mathrm{e} = N_\mathrm{e}/N_\mathrm{H}$, as a function of redshift. Because of the particle conservation and the number of electrons in excited states of H I and He I being negligible, one may write[3]

$$N_\mathrm{e} \approx N_\mathrm{H}(1 - X^\mathrm{H}_\mathrm{1s}) + N_\mathrm{H}(f_\mathrm{He} - X^\mathrm{He}_\mathrm{1s}), \tag{1}$$

where N_H denotes the number density of hydrogen nuclei, and $f_\mathrm{He} = N_\mathrm{He}/N_\mathrm{H}$ is the fraction of helium nuclei. The populations of the different levels are given by $X^\mathrm{a}_i = N^\mathrm{a}_i/N_\mathrm{H}$, where 'a' indicates the atomic species. Furthermore, $X_i \equiv X^\mathrm{H}_i$ for convenience.

Equation (1) implies that the recombination problem reduces to finding solutions to X^a_1s. For hydrogen, the *standard* rate equation describing the evolution of the ground-state population has the form (see also Seager et al. 1999, 2000)

$$\left.\frac{\mathrm{d}X^\mathrm{H}_\mathrm{1s}}{\mathrm{d}t}\right|_\mathrm{st} = \Delta R^\mathrm{st}_{2\mathrm{s}\leftrightarrow 1\mathrm{s}} + \sum_k \Delta R^\mathrm{st}_{k\mathrm{p}\leftrightarrow 1\mathrm{s}}, \tag{2a}$$

$$\Delta R^\mathrm{st}_{2\mathrm{s}\leftrightarrow 1\mathrm{s}} = A_{2\mathrm{s}1\mathrm{s}}\left(X^\mathrm{H}_\mathrm{2s} - X^\mathrm{H}_\mathrm{1s}\mathrm{e}^{-h\nu_{21}/kT_\gamma}\right), \tag{2b}$$

$$\Delta R^\mathrm{st}_{k\mathrm{p}\leftrightarrow 1\mathrm{s}} = A_{k\mathrm{p}1\mathrm{s}}(1 + n^\mathrm{pl}_{k\mathrm{p}1\mathrm{s}})\left(X^\mathrm{H}_{k\mathrm{p}} - 3\,X^\mathrm{H}_\mathrm{1s}\bar{n}_{k\mathrm{p}1\mathrm{s}}\right). \tag{2c}$$

Here, $\bar{n}_{k\mathrm{p}1\mathrm{s}}$ is the mean photon occupation number over the Lyman-k line profile, A_i is the atomic rate coefficients for spontaneous emission and $n^\mathrm{pl}_{k\mathrm{p}1\mathrm{s}}$ is the occupation number of the CMB blackbody photons at the Lyman-k transition frequency $\nu_{k1} \equiv \nu_{k\mathrm{p}1\mathrm{s}}$.

The solution of equation (2) depends on the level populations of the 2s and *k*p states. In addition, the photon distribution in the vicinity of every Lyman resonance has to be known to define $\bar{n}_{k\mathrm{p}1\mathrm{s}}$. $\bar{n}_{k\mathrm{p}1\mathrm{s}}$ is often estimated by the Sobolev approximation, which, however, breaks down during recombination, leading to non-negligible corrections to the recombination dynamics (e.g. see Chluba & Sunyaev 2009a,b, 2010b). The rate equations for the 2s and *k*p states themselves can, in principle, be explicitly given. But here it is only important to realize that these lead to a large network of rate equations which depend on the populations of *all other* excited levels. To further complicate matters, the electron temperature, T_e, enters the whole problem via recombination coefficients, $\alpha_i(T_\mathrm{e}, T_\gamma)$, to each level i, where T_γ is the photon temperature.

The evolution of T_e is described by one simple differential equation, which accounts for the cooling of electrons caused by the Hubble expansion, and the energy exchange with CMB photons via Compton scattering. Other processes, e.g. bremsstrahlung cooling, are subdominant (Seager et al. 2000).

2.1.1 *The effective multilevel approach*

Recently, Ali-Haïmoud & Hirata (2010) suggested to simplify the recombination problem to a subset of levels that need to be followed explicitly. Here, we shall call the members of this subset 'resolved' levels. This approach enables us to account for the effect of recombinations due to highly excited states ($n > 100$), without actually solving for all these level populations explicitly. The rationale being that except for the optically thick Lyman-series transitions, all other rates are mediated by the CMB blackbody photons, and hence only depend on the photon and electron temperatures.

The downside of this simplification entails the need to tabulate *effective* rate coefficients as a function of T_γ and T_e prior to the computation. This, however, needs to be done only once, and given that the number of resolved states necessary for converging solutions is small, this *effective multilevel approach* results in tremendous

[2] This code will be available at www.Chluba.de/CosmoRec.

[3] We assume to be at redshifts $z \ll 6000$, well after doubly ionized helium recombines.

speedup for recombination calculations (see Ali-Haïmoud & Hirata 2010, for more details). For this work, we also implemented an effective rate approach. The rate coefficients for an effective 400-shell hydrogen atom were computed using our most recent recombination code (Chluba et al. 2010), while helium is described with a multilevel treatment (Chluba & Sunyaev 2010a).

Within this framework, the choice of the number of resolved states depends on the extra *physics* that one intends to include. For example, in a *minimal* model for the hydrogen recombination problem, one should explicitly solve for the 1s, 2s and 2p level populations in tandem with the electron temperature, $T_{\rm e}$.[4]

This minimal choice already allows us to include processes that affect the net rates in the 2s–1s two-photon channel and the 2p–1s Lyman α resonance, e.g. the effect of stimulated 2s–1s two-photon decay (Chluba & Sunyaev 2006b) or the feedback of Lyman α photons on the 1s–2s rate (Kholupenko & Ivanchik 2006). However, since we restricted ourselves to the 1s, 2s and 2p states, corrections due to Lyman β or higher resonance feedback cannot be modelled as these would require resolving np states with $n > 2$ (Chluba & Sunyaev 2007). We will return to these points in Section 2.2.1.

2.1.2 *Sobolev approximation for $\bar{n}_{k\rm p1s}$*

In a multilevel approach, the Sobolev approximation is invoked to obtain a solution for the photon field around every resonance appearing in equation (2c). The photon occupation number around each line is then given by[5]

$$\Delta n_\nu^k = \Delta n_{\rm L}^k \left[1 - {\rm e}^{-\tau_{\rm S}^k (1-\chi_\nu^k)}\right], \tag{3}$$

where $\Delta n_{\rm L}^k \approx n_{\rm L}^k - n_{k\rm p1s}^{\rm pl}$, $\tau_{\rm S}^k$ is the Sobolev optical depth in the Lyman-k resonance, and $\chi_\nu^k = \int_0^\nu \varphi_{\rm V}^k(\nu)\,{\rm d}\nu$. Here, $\varphi_{\rm V}^k(\nu)$ is the Voigt profile corresponding to a resonance, and the line occupation number, $n_{\rm L}^k$, is defined as

$$n_{\rm L}^k = \frac{N_{k\rm p}}{3\,N_{1\rm s}}. \tag{4}$$

Consequently, a simple approximation for the mean occupation number is

$$\bar{n}_{k\rm p1s} = n_{\rm L}^k - P_{\rm S}^k \Delta n_{\rm L}^k \tag{5}$$

with $P_{\rm S}^k = (1 - {\rm e}^{-\tau_{\rm S}^k})/\tau_{\rm S}^k$ being the Sobolev escape probability.

For the Lyman α resonance, equation (3) results in a photon distribution that is rather unphysical (e.g. see discussion in Chluba & Sunyaev 2009b). This is primarily due to the assumption that every interaction with the resonance leads to a complete redistribution of photons over the whole line profile, which for typical values of $\tau_{\rm S}$ during recombination couples the photon distribution from the line centre up to frequencies in the Lyman continuum. For the conditions present in our Universe, photon redistribution over frequency is much less effective, most notably in the distant wings. Thus, it is important to distinguish between scattering, real emission and absorption events, as we will discuss in Section 3.

[4] Because the 2s and 2p states are usually close to full statistical equilibrium, one could also eliminate either of these states using $X_{2\rm p} = 3X_{2\rm s}$ and, as a result, closely resemble the normal RECFAST code, now without requiring a fudge factor.

[5] We assumed that as $\nu \rightarrow \infty$, the distortion $\Delta n_\infty \rightarrow 0$, and that (as usual) the factor of $(\nu_{k1}/\nu)^2 \sim 1$.

2.2 Beyond the standard rate equation for 1s

As mentioned in Section 2.1.1 within the effective multilevel approach, the choice for the resolved states depends on the physics to be modelled in detail. For example, in order to include the full effect of Lyman-series feedback, say up to $n = 8$, the *minimal* model that follows 1s, 2s and 2p would at least have to be extended by all kp states up to 8p state.

Also, the inclusion of two-photon processes from higher levels and Raman scattering requires us to rewrite equation (2) in a more generalized form as

$$\left.\frac{{\rm d}X_{1\rm s}^{\rm H}}{{\rm d}t}\right|_{\rm mod} = \sum_i \left(X_i^{\rm H} R_{i\rightarrow 1\rm s} - X_{1\rm s}^{\rm H} R_{1\rm s\rightarrow i}\right), \tag{6}$$

where $R_{i\rightarrow j}$ are the rates between the levels i and j. These rates depend on atomic physics, the CMB blackbody, the electron temperature and the solution for the Lyman-series spectral distortion introduced by the recombination process.

To include two-photon corrections to the Lyman series up to $n \leq n_{\rm max}$, the important levels to follow are all the nd and ns states with $2 \leq n \leq n_{\rm max}$. The corresponding partial rates to the np states drop out of the equations, and the Lyman-series emission and absorption profiles, usually given by a Voigt function, will be replaced by the two-photon profiles for the ns $\leftrightarrow$ 1s and nd $\leftrightarrow$ 1s processes, and similarly for the Raman process. We will specify these corrections more precisely in the following sections.

2.2.1 *Accounting for corrections from radiative transfer effects*

Changes in the level populations, electron temperature and free electron fraction remain small ($\sim$1 per cent), when different physical processes, which were neglected in earlier treatments (e.g. see Rubiño-Martín et al. 2010, for overview), are included. This justifies treating corrections to $T_{\rm e}$ and the populations of resolved levels, X_i, as small *perturbations*. On the other hand, it has been shown that the changes in the photon field caused by time-dependence (Chluba & Sunyaev 2009b), line scattering (Chluba & Sunyaev 2009a; Hirata & Forbes 2009) or two-photon corrections (Hirata 2008; Chluba & Sunyaev 2010b) are *non-perturbative*.

In Section 3, we derive in detail the different correction terms for the photon diffusion equation and provide modifications to the net rates of the effective multilevel atom. The idea is to first solve the recombination history using the effective multilevel approach in the '1 + 1'-photon description, i.e. equate $R_{i\rightarrow j} = R_{i\rightarrow j}^{1+1}$ in equation (6), and then compute the solution to the photon field using the radiative transfer equation. This then leads to corrections in the net rates, which are used in computing changes to the recombination dynamics, and hence modify equation (6). These corrections being small demand only one iteration to converge. Detailed descriptions to the notations in the following sections and part of the methods used can also be found in Chluba & Sunyaev (2009a,b, 2010b).

3 EQUATION FOR THE PHOTON FIELD EVOLUTION AND CORRECTIONS TO THE EFFECTIVE MULTILEVEL ATOM

To account for all corrections to the cosmological recombination problem, it is important to follow the evolution of *non-thermal photons* in the Lyman series, which are produced during recombination. These photons interact strongly with neutral hydrogen atoms throughout the entire epoch of recombination, and their rate of

escape from the Lyman resonances is one of the key ingredients in accurately solving the recombination problem.

The partial differential equation governing the evolution of the photon field has the form (see Chluba & Sunyaev 2009b, for a detailed discussion)

$$\frac{1}{c}\left(\left.\frac{\partial \Delta n_\nu}{\partial t}\right|_\nu - H\nu \left.\frac{\partial \Delta n_\nu}{\partial \nu}\right|_t\right) = \mathcal{C}(\Delta n_\nu)_{\rm em/abs} + \mathcal{C}(\Delta n_\nu)_{\rm scat}, \quad (7)$$

where $\Delta n_\nu = [c^2/(2\nu^2)]\Delta N_\nu$ is the distortion in the photon occupation number, and a distinction is made between the collision terms leading to emission and absorption, $\mathcal{C}(\Delta n_\nu)_{\rm em/abs}$, and scattering, $\mathcal{C}(\Delta n_\nu)_{\rm scat}$. As an example, the first term on the right-hand side of the equation can account for two-photon corrections to the line profiles, while the second term accounts for electron and/or resonance scattering. The second term on the left-hand side describes the redshifting of photons due to Hubble expansion, and plays a crucial role in the escape of photons from the optically thick Lyman-series resonances.

In equation (7), the CMB blackbody has been subtracted, i.e. $\Delta n_\nu = n_\nu - n_\nu^{\rm pl}$, where $n_\nu^{\rm pl} = (\mathrm{e}^{h\nu/kT_\gamma} - 1)^{-1}$ is the blackbody occupation number, because the left-hand side directly vanishes for a blackbody with temperature $T_\gamma(z) \propto (1+z)$. Also, spectral distortions created by Compton scattering of electrons with $T_\mathrm{e} \neq T_\gamma$ will be extremely small for conditions in our Universe,[6] at least if there is no additional energy release.

By changing the time variable to redshift z using $\mathrm{d}z/\mathrm{d}t = -H(1+z)$, and scaling to dimensionless frequency $x = \nu/\nu_{21}$, equation (7) reads

$$\left.\frac{\partial \Delta n_x}{\partial z}\right|_x = -\frac{x}{(1+z)}\left.\frac{\partial \Delta n_x}{\partial x}\right|_z - \Lambda_z\left\{\mathcal{C}(\Delta n_\nu)_{\rm em/abs} + \mathcal{C}(\Delta n_\nu)_{\rm scat}\right\}, \quad (8)$$

where $\Delta n_x = \nu_{21}\,\Delta n_\nu$ and $\Lambda_z = c\nu_{21}/[H(1+z)]$. We will now discuss the terms describing the resonance and electron scattering. In Section 3.1, we specify the different emission and absorption terms, which then in Sections 4 and 5 are used to compute the corrections to the Lyman-series distortion and ionization history.

3.1 Inclusion of partial redistribution by resonance and electron scattering

Here, we provide the terms for the Boltzmann equation describing the effect of (partial) photon redistribution by resonance and electron scattering. The form of the collision term for these cases within a Fokker–Planck formulation was discussed earlier (e.g. Zeldovich & Sunyaev 1969; Basko 1978b,a; Rybicki & dell'Antonio 1994; Sazonov & Sunyaev 2000; Rybicki 2006; Chluba & Sunyaev 2009a). Since we are only following the evolution of the distortion from a blackbody, and since it is clear that induced effects are negligible,[7] one can readily write as

$$\Lambda_z\,\mathcal{C}(\Delta n_\nu)|_{\rm scatt} \approx \frac{1}{x^2}\frac{\partial}{\partial x}\,\mathcal{D}(x)\left[\frac{\partial}{\partial x}\Delta n_x + \xi(z)\Delta n_x\right], \quad (9)$$

where x is the dimensionless frequency and $\xi(z) = \frac{h\nu_{21}}{kT_\mathrm{e}} \approx 40\,\frac{1100}{(1+z)}$. The first term on the right-hand side describes photon diffusion and the second term accounts for the recoil effect.

3.1.1 Electron scattering

The diffusion coefficient in the case of electron scattering is (e.g. see Zeldovich & Sunyaev 1969; Sazonov & Sunyaev 2000)

$$\mathcal{D}_\mathrm{e}(x) = \frac{\sigma_\mathrm{T} N_\mathrm{e} c}{H(1+z)}\left(\frac{kT_\mathrm{e}}{m_\mathrm{e}c^2}\right)x^4, \quad (10)$$

where $\sigma_\mathrm{T} \approx 6.65\times10^{-25}\,\mathrm{cm}^2$ is the Thomson cross-section. Chluba & Sunyaev (2009a) pointed out that electron scattering has an effect only at the early stages of recombination ($z \gtrsim 1400$). However, it is easy to include, and also has the advantage of stabilizing the numerical treatment by damping small-scale fluctuations of the photon occupation number caused by numerical errors, even in places where line scattering is already negligible.

As can be seen from the form of the diffusion coefficient in equation (10), the efficiency of electron scattering to a large extent is *achromatic*. This is in stark contrast to the case of resonance scattering, which is most efficient only in a very narrow range around the line centre (see the next paragraph). Furthermore, the number of free electrons drops rapidly towards the end of recombination, such that the Fokker–Planck approximation is expected to break down (Chluba & Sunyaev 2009a). Nevertheless, the diffusion approximation remains sufficient for computations of the free electron fraction (see Ali-Haïmoud, Grin & Hirata 2010).

3.1.2 Resonance scattering

For resonance scattering by a Lyman-k line, the diffusion coefficient is (e.g. see Basko 1978b,a; Rybicki 2006; Chluba & Sunyaev 2009a, and reference therein)

$$\mathcal{D}_k(x) \approx p_\mathrm{sc}^{k\mathrm{p}}\,\frac{\sigma_\mathrm{r}^{k\mathrm{p}} N_{1\mathrm{s}} c}{H(1+z)}\left(\frac{kT_\mathrm{e}}{m_\mathrm{H}c^2}\right)\frac{\nu_{k1}^2}{\nu_{21}^2}x^2\phi_\mathrm{V}^{k\mathrm{p}}(x), \quad (11)$$

where $\sigma_\mathrm{r}^{k\mathrm{p}} = \frac{3\lambda_{k1}^2}{8\pi}\frac{A_{k\mathrm{p}1\mathrm{s}}}{\Delta\nu_\mathrm{D}^{k\mathrm{p}}}$ and $\Delta\nu_\mathrm{D}^{k\mathrm{p}}$ denote the resonant-scattering cross-section and the Doppler width of the Lyman-k resonance, respectively. For the Lyman α line, $\sigma_\mathrm{r}^{2\mathrm{p}} \sim 1.91\times10^{-13}\,\mathrm{cm}^2$ and $\Delta\nu_\mathrm{D}^{2\mathrm{p}} \sim 2.35\times10^{-5}\;\nu_{21}$ at $z\sim1100$. The Voigt profile, $\phi_\mathrm{V}^{k\mathrm{p}}(x) = \varphi_\mathrm{V}^{k\mathrm{p}}(x)\,\Delta\nu_\mathrm{D}^{k\mathrm{p}}$, is normalized as $\int_{-\infty}^{\infty}\phi_\mathrm{V}^{k\mathrm{p}}(x_\mathrm{D}^{k\mathrm{p}})\,\mathrm{d}x_\mathrm{D}^{k\mathrm{p}} = \int_0^\infty\varphi_\mathrm{V}^{k\mathrm{p}}(\nu)\,\mathrm{d}\nu = 1$, where $x_\mathrm{D}^{k\mathrm{p}} = (\nu-\nu_{k\mathrm{p}})/\Delta\nu_\mathrm{D}^{k\mathrm{p}}$ is the distance to the line centre in units of the Doppler width.

The scattering probability of the Lyman-k resonance, $p_\mathrm{sc}^{k\mathrm{p}}$, is determined by a *weighted count* of all possible ways *out* of the kp state, $R_{k\mathrm{p}}^-(T_\gamma)$, excluding the Lyman-series resonance being considered, and then writing the branching ratio as[8]

$$p_\mathrm{sc}^{k\mathrm{p}} = \frac{A_{k\mathrm{p}1\mathrm{s}}}{A_{k\mathrm{p}1\mathrm{s}} + R_{k\mathrm{p}}^-}, \quad (12)$$

yielding the probability for re-injection into the Lyman-k resonance. The rates $R_{k\mathrm{p}}^-(T_\gamma)$ and the scattering probabilities, $p_\mathrm{sc}^{k\mathrm{p}}(T_\gamma)$, can be pre-computed, independent of the solutions obtained from the multilevel code. We detail the procedure below.

Following Rybicki & dell'Antonio (1994), the diffusion coefficient is $D \propto \phi_\mathrm{V}^{k\mathrm{p}}(\nu)$. We neglect corrections due to non-resonant

[6] The cooling of CMB photons by losing energy to keep electrons at $T_\mathrm{e} \sim T_\gamma$ should lead to a y-distortion with y-parameter $y \sim 10^{-10}$ to 10^{-9}. The dissipation of energy by acoustic waves should lead to $y \sim 10^{-8}$. These can be neglected for our purpose.

[7] Eliminating the dominant term of the CMB blackbody leaves us with a term that is tiny because we are always in the distant Wien tail of the CMB at all times during recombination.

[8] Stimulated emission for the Lyman series has been neglected.

contributions (e.g. see Lee 2005) in calculating the scattering cross-section, which would lead to a different frequency dependence far away from the resonance (e.g. Rayleigh scattering in the distant red wing, Jackson 1998). However, because it turns out that resonance scattering is only important in the vicinity of the Lyman α resonance, this approximation suffices.

It is also worth mentioning that equation (11) together with equation (9), in the limit of large optical depth,[9] provides a viable description for the redistribution of photon over frequency. Unlike the case of *complete redistribution* (in which the re-emission after each scattering event occurs over the whole Voigt profile) in the recombination epoch, photons are only *partially redistributed* as a result of the Doppler motions of the hydrogen atoms, so-called type II redistribution as defined in Hummer (1962).

3.1.3 Equilibrium solution for the scattering term

Independent of the type of scattering, the equilibrium distribution with respect to the scattering term equation (9) is given by

$$\Delta n_x^{\rm sc,eq} = \Delta n_{x_0}(z)\, {\rm e}^{-\xi(z)(x-x_0)}. \tag{13}$$

This is the expected Wien spectrum with the temperature defined by the electrons. The normalization $\Delta n_{x_0}(z)$ is determined by the emission and absorption process.

The optical depth to line scattering being extremely large inside the Doppler cores of the Lyman resonances ($\tau_{\rm S} \sim 10^6$–10^8 during H I recombination) causes the photon distribution within the Doppler core to remain extremely close to equilibrium, $\Delta n_x^{\rm sc,eq}$.

3.2 Normal Lyman-*k* emission and absorption terms

In the normal '1 + 1'-photon picture, the emission profile for each Lyman-series resonance is given by a Voigt profile, $\varphi_{\rm V}^{k{\rm p}}$, with Voigt parameter $a^{k{\rm p}}$. Given the rate, $R_{k{\rm p}}^{+}(T_\gamma, T_{\rm e})$, at which *fresh*[10] electrons reach the kp state, and the probability of photon injection into the Lyman-k resonance, $p_{\rm em}^{k{\rm p}} \equiv p_{\rm sc}^{k{\rm p}}$, the Lyman-$k$ line emission and absorption term are (e.g. see Chluba & Sunyaev 2010b) written as

$$\left.\frac{\partial \Delta n_x}{\partial z}\right|_{\rm em/abs}^{{\rm Ly}-k} = -p_{\rm d}^{k{\rm p}}\, \frac{\sigma_{\rm r}^{k{\rm p}} N_{1{\rm s}} c}{H(1+z)}\, \frac{\nu_{k1}^2}{\nu_{21}^2}\, \frac{\phi_{\rm V}^{k{\rm p}}}{x^2}\, \left(\nu_{2{\rm p}1{\rm s}}\, \Delta n_{\rm em}^{k{\rm p}} - f_x^{k{\rm p}} \Delta n_x\right). \tag{14}$$

The factor of $1/x^2$ accounts for the translation from photon number to the occupation number because $\Delta N_\nu \propto \nu^2 \Delta n_\nu$, for which the Voigt profile is defined. Also, $p_{\rm d}^{k{\rm p}} = 1 - p_{\rm em}^{k{\rm p}}$ is the death or the real absorption probability in the kth Lyman-series resonance, and $\Delta n_{\rm em}^{k{\rm p}}$ and $f_x^{k{\rm p}}$ are given by

$$\Delta n_{\rm em}^{k{\rm p}} = \frac{g_{1{\rm s}}}{g_{k{\rm p}}}\, \frac{R_{k{\rm p}}^{+}}{R_{k{\rm p}}^{-} N_{1{\rm s}}} - {\rm e}^{-h\nu_{k1}/kT_\gamma}, \tag{15a}$$

$$f_x^{k{\rm p}} = \exp\left[h(\nu-\nu_{k1})/kT_\gamma\right], \tag{15b}$$

where $g_{1{\rm s}}/g_{k{\rm p}}$ is the ratio of the statistical weights of the initial and final states. The function $\Delta n_{\rm em}^{k{\rm p}}(T_\gamma, T_{\rm e})$ can, in principle, be pre-computed using the solution for the populations of the levels from the initial run of the effective multilevel recombination code.

[9] During hydrogen recombination, photons scatter efficiently off the Lyman α resonance out to $\sim 10^4$–10^5 Doppler width (see fig. 3 in Chluba & Sunyaev 2009b). However, the redistribution of photons in the distant damping wings still remains rather slow (Chluba & Sunyaev 2009a).

[10] Electrons that did not enter the p state via the Lyman-k resonance.

However, the simplest way to define the ratio $R_{k{\rm p}}^{+}/R_{k{\rm p}}^{-}$ is to use the quasi-stationary approximation for the np-population (see the details below). We also note that in full thermodynamic equilibrium $\Delta n_{\rm em}^{k{\rm p}} = 0$, so that no distortion is created ($\Delta n_x = 0$).

Physically, equation (14) includes two important aspects, which are not considered in the standard recombination calculation. First, it allows for a distinction between scattering events on one side, and real emission and absorption events on the other side. Secondly, it ensures conservation of blackbody spectrum in full thermodynamic equilibrium, even in the very distant wings of the lines. Refer to Chluba & Sunyaev (2010b) for a detailed explanation of the latter point, and on how this leads to one of the largest corrections in the case of Lyman α transport.

3.2.1 Computing $\Delta n_{\rm em}^{k{\rm p}}$

To solve the evolution of the photon field, one has to know at which rate photons are produced by the Lyman resonance. This rate depends on $\Delta n_{\rm em}^{k{\rm p}}$ as defined in equation (15).

The rate equation for the evolution of the population in the kp level has the form (see Appendix B; Chluba & Sunyaev 2010b)

$$\frac{{\rm d}X_{k{\rm p}}}{{\rm d}t} = \left.\frac{{\rm d}X_{k{\rm p}}}{{\rm d}t}\right|_{{\rm Ly}-k} + R_{k{\rm p}}^{+} - R_{k{\rm p}}^{-} X_{k{\rm p}}, \tag{16a}$$

$$\left.\frac{{\rm d}X_{k{\rm p}}}{{\rm d}t}\right|_{{\rm Ly}-k} = \frac{g_{1{\rm s}}}{g_{k{\rm p}}} A_{k{\rm p}1{\rm s}}\, X_{1{\rm s}}\, \mathcal{I}_1^{k{\rm p}} - A_{k{\rm p}1{\rm s}}\, X_{k{\rm p}} \mathcal{I}_2^{k{\rm p}}, \tag{16b}$$

$$\mathcal{I}_1^{k{\rm p}} = \int \varphi_{\rm V}^{k{\rm p}}(\nu)\, {\rm e}^{h(\nu-\nu_{k1})/kT_\gamma}\, n_\nu\, {\rm d}\nu, \tag{16c}$$

$$\mathcal{I}_2^{k{\rm p}} = \int \varphi_{\rm V}^{k{\rm p}}(\nu)(1+n_\nu)\, {\rm d}\nu \approx 1 + n^{\rm pl}(\nu_{k1}) \approx 1. \tag{16d}$$

In this picture, the emission, absorption and resonance scattering terms are all treated simultaneously. In addition, the asymmetry between the emission and the absorption profile in the Lyman-k resonance, as required by detailed balance, has been incorporated.

Under quasi-stationarity, and using the definition of the death probability, $p_{\rm d}^{k{\rm p}}$, equation (16) yields

$$\frac{g_{1{\rm s}}}{g_{k{\rm p}}}\, \frac{R_{k{\rm p}}^{+}}{R_{k{\rm p}}^{-} X_{1{\rm s}}} = \frac{1}{p_{\rm d}^{k{\rm p}}} \left(\frac{g_{k{\rm p}}}{g_{1{\rm s}}}\, \frac{X_{k{\rm p}}}{X_{1{\rm s}}} - \mathcal{I}_1^{k{\rm p}}\right) + \mathcal{I}_1^{k{\rm p}}, \tag{17}$$

such that with equation (15)

$$\Delta n_{\rm em}^{k{\rm p}} = \frac{1}{p_{\rm d}^{k{\rm p}}} \left(\frac{g_{k{\rm p}}}{g_{1{\rm s}}}\, \frac{X_{k{\rm p}}}{X_{1{\rm s}}} - \mathcal{I}_1^{k{\rm p}}\right) + \mathcal{I}_1^{k{\rm p}} - {\rm e}^{-h\nu_{k{\rm p}1{\rm s}}/kT_\gamma} \tag{18a}$$

$$\approx \Delta n_{\rm L}^{k} \left(1 + \frac{p_{\rm em}^{k{\rm p}}}{p_{\rm d}^{k{\rm p}}}\, P_{\rm S}^{k}\right). \tag{18b}$$

In the second step, we used the normal Sobolev approximation, for which $\mathcal{I}_1^{k{\rm p}} \approx n_{\rm L}^{k} - P_{\rm S}^{k}(n_{\rm L}^{k} - n_{k{\rm p}1{\rm s}}^{\rm pl})$ (for the case of Lyman α compare also with equation (41) in Chluba & Sunyaev 2009b).

From equation (18b), we have $\Delta n_{\rm em}^{k{\rm p}} \approx \Delta n_{\rm L}^{k}$, since for all Lyman-series resonances the second term in brackets is very small. Nevertheless, for the total normalization of the line intensity close to the line centre, this small correction is important (Chluba & Sunyaev 2009b), in particular for the Lyman α resonance.

Also we would like to mention that for the Voigt parameter of the Lyman-k profiles, $a^{k{\rm p}} = A_{\rm tot}^{k{\rm p}}/(4\pi\Delta\nu_{\rm D}^{k{\rm p}})$, the *total* width of the line is used, where transitions induced by the CMB blackbody (e.g. to

higher levels) are included. Numerically, it is possible to compute the total width for the Lyman-k resonance with $A^{\rm kp}_{\rm tot} \equiv A_{k{\rm p}1{\rm s}}/p^{\rm kp}_{\rm em}$.

3.3 The 2s–1s two-photon channel

The 2s–1s two-photon channel provides the pathway for about 60 per cent of all electrons in hydrogen to settle into the ground state (Chluba & Sunyaev 2006a). Therefore, it provides the most important channel in the cosmological recombination process. Here, we treat the case of 2s–1s separately to illustrate the important approximations in the two-photon picture. The derivation outlined in this section is then used to obtain the corresponding terms for the two-photon processes from excited states with $n > 2$ (see Section 3.4).

The net change of the number density of electrons in the 2s level via the 2s–1s two-photon channel is given by

$$\left.\frac{{\rm d}X_{\rm 2s}}{{\rm d}t}\right|^{2\gamma}_{\rm 1s} = A^{2\gamma}_{\rm 2s1s} X_{\rm 1s} \int \varphi^{2\gamma}_{\rm 2s}\, n(\nu)\, n(\nu_{21}-\nu)\, {\rm d}\nu - A^{2\gamma}_{\rm 2s1s} X_{\rm 2s} \int \varphi^{2\gamma}_{\rm 2s}\, [1+n(\nu)][1+n(\nu_{21}-\nu)]\, {\rm d}\nu, \tag{19}$$

where $A^{2\gamma}_{\rm 2s1s} = 8.2206\ {\rm s}^{-1}$ (Labzowsky, Shonin & Solovyev 2005) is the vacuum 2s–1s two-photon decay rate, and $\varphi^{2\gamma}_{\rm 2s}$ denotes the 2s–1s two-photon decay profile normalized as $\int \varphi^{2\gamma}_{\rm 2s}\, {\rm d}\nu = 1$. Including all possible ways in and out of the 2s level, the net change of the number density of electrons in the 2s state can be written as

$$\frac{{\rm d}X_{\rm 2s}}{{\rm d}t} = \left.\frac{{\rm d}X_{\rm 2s}}{{\rm d}t}\right|^{2\gamma}_{\rm 1s} + R^{+}_{\rm 2s} - R^{-}_{\rm 2s} X_{\rm 2s}. \tag{20}$$

Here, $R^{+}_{\rm 2s}$ and $R^{-}_{\rm 2s}$ include the effect of all transitions to bound states with $n > 2$ and the continuum.

In order to simplify the notation, we now introduce

$$\langle\, f(\nu)\,\rangle^{2\gamma}_{i} = \int_0^{\nu_{i1{\rm s}}} \varphi^{2\gamma}_{i}\, f(\nu)\, {\rm d}\nu, \tag{21a}$$

$$\mathcal{G}^{i}_{1} = \langle\, n\, n'\,\rangle^{2\gamma}_{i}, \tag{21b}$$

$$\mathcal{G}^{i}_{2} = \langle\, (1+n)(1+n')\,\rangle^{2\gamma}_{i}, \tag{21c}$$

where $f(\nu)$ is some arbitrary function of frequency and $n = n(\nu)$ and $n' = n(\nu')$ with $\nu' = \nu_{i1{\rm s}} - \nu$.

Then, under *quasi-stationarity*, the solution for the population of the 2s state is given by

$$X^{\rm QS}_{\rm 2s} = \frac{R^{+}_{\rm 2s} + A^{2\gamma}_{\rm 2s1s} X_{\rm 1s}\, \mathcal{G}^{\rm 2s}_{1}}{R^{-}_{\rm 2s} + A^{2\gamma}_{\rm 2s1s}\, \mathcal{G}^{\rm 2s}_{2}}. \tag{22}$$

In the multilevel approach, the effect of stimulated two-photon emission is neglected leading to $\mathcal{G}^{\rm 2s}_{2} \approx 1$. Also any CMB spectral distortion that is introduced by the recombination process (e.g. because of Lyman α emission) is omitted, implying $\mathcal{G}^{\rm 2s}_{1} \approx \langle\, n^{\rm pl}\, n^{\rm pl'}\,\rangle^{2\gamma}_{\rm 2s} \approx \exp(-h\nu_{21}/kT_\gamma)$. In this approximation, the result from equation (22) becomes identical to the one obtained using equations (2b) and (20), in the standard multilevel approach.

However, in the recombination problem, corrections to both $\mathcal{G}^{\rm 2s}_{1}$ and $\mathcal{G}^{\rm 2s}_{2}$ are important. For the stimulated two-photon emission, only the occupation number given by the undistorted CMB blackbody has to be considered and thus,

$$\mathcal{G}^{\rm 2s}_{2} \approx \langle\, (1+n^{\rm pl})(1+n^{\rm pl'})\,\rangle^{2\gamma}_{\rm 2s} \equiv \mathcal{G}^{\rm 2s,pl}_{2}, \tag{23}$$

which can be pre-computed as a function of temperature. Typically, $\mathcal{G}^{\rm 2s,pl}_{2}$ exceeds unity by a few per cent (Chluba & Sunyaev 2006b).

For $\mathcal{G}^{\rm 2s}_{1}$, one can make use of the fact that the distortions at either ν or ν' are very small, so that

$$n\, n' \approx n^{\rm pl}\, n^{\rm pl'} + n^{\rm pl'}\, \Delta n + n^{\rm pl}\, \Delta n'. \tag{24}$$

Hence equation (19) can be rewritten as

$$\left.\frac{{\rm d}X_{\rm 2s}}{{\rm d}t}\right|^{2\gamma}_{\rm 1s} = A^{2\gamma,*}_{\rm 2s1s}\left(X_{\rm 1s}{\rm e}^{-h\nu_{21}/kT_\gamma} - X_{\rm 2s}\right) + A^{2\gamma}_{\rm 2s1s}\, X_{\rm 1s}\, \Delta\mathcal{G}^{\rm 2s}_{1}, \tag{25a}$$

$$\Delta\mathcal{G}^{\rm 2s}_{1} = \int \varphi^{2\gamma}_{\rm 2s}\left(n^{\rm pl'}\Delta n + n^{\rm pl}\,\Delta n'\right)\, {\rm d}\nu \equiv 2\int_{\frac{\nu_{21}}{2}}^{\nu_{21}} \varphi^{2\gamma}_{\rm 2s}\, n^{\rm pl'}\Delta n\, {\rm d}\nu, \tag{25b}$$

where we defined the stimulated 2s–1s two-photon decay rate within the CMB ambient radiation field as $A^{2\gamma,*}_{\rm 2s1s} = A^{2\gamma}_{\rm 2s1s}\, \mathcal{G}^{\rm 2s,pl}_{2}$ (cf. Chluba & Sunyaev 2006b). Also equation (25b) reflects the symmetry of the two-photon profile around $\nu = \nu_{21}/2$.

Note that for $\mathcal{G}^{\rm 2s,pl}_{2}$, only the CMB blackbody spectrum is important and therefore can, in principle, be pre-computed as a function of photon temperature, T_γ. This also emphasizes the difference in the origin of the two terms of equation (25a), $\mathcal{G}^{\rm 2s,pl}_{2}$ being the *thermal* contribution, while $\Delta\mathcal{G}^{\rm 2s}_{1}$ arises solely because of *non-thermal* photons created in the recombination process.

By comparing equation (25) with equation (2b), one can write down the correction to the 2s–1s net two-photon rate

$$\Delta R^{\rm corr}_{\rm 2s\leftrightarrow 1s} = A^{2\gamma}_{\rm 2s1s}\Delta\mathcal{G}^{\rm 2s,pl}_{2}\left(X_{\rm 1s}{\rm e}^{-h\nu_{21}/kT_\gamma} - X_{\rm 2s}\right) + A^{2\gamma}_{\rm 2s1s}\, X_{\rm 1s}\, \Delta\mathcal{G}^{\rm 2s}_{1}. \tag{26}$$

Here, we introduced $\Delta\mathcal{G}^{\rm 2s,pl}_{2} = \mathcal{G}^{\rm 2s,pl}_{2} - 1$, which during recombination is of the order of $\sim$1 per cent. In equation (25), the integral $\Delta\mathcal{G}^{\rm 2s}_{1}$ depends on the spectral distortion introduced by the recombination process in the Wien's tail of the CMB blackbody. Including only the Lyman α distortion provides a manner in which to take its feedback effect into account (cf. Kholupenko & Ivanchik 2006).

3.3.1 The 2s–1s two-photon emission and absorption term

In contrast to the Lyman-series channels, the terms for the photon radiative transfer equation in the case of the 2s–1s channel can be directly obtained from the net rate between the 2s and 1s state as in equation (19), resulting in

$$\frac{1}{c}\frac{\partial N_\nu}{\partial t}\bigg|^{\rm 2s1s}_{2\gamma} = A^{2\gamma}_{\rm 2s1s} N_{\rm 2s}\tilde{\varphi}^{2\gamma}_{\rm 2s}[1+n(\nu)][1+n(\nu_{21}-\nu)] - A^{2\gamma}_{\rm 2s1s} N_{\rm 1s}\tilde{\varphi}^{2\gamma}_{\rm 2s}\, n(\nu)\, n(\nu_{21}-\nu). \tag{27}$$

Here, we defined $\tilde{\varphi}^{2\gamma}_{\rm 2s} = \frac{2\,\varphi^{2\gamma}_{\rm 2s}}{4\pi}$, where the factor of 2 results from two photons being added to the photon field, and the 4π converts the units to per steradian.

The reason for this simple connection to the net rate equation is related to the fact that every transition from the 1s state to the 2s level is expected to lead to a *complete redistribution* over the 2s–1s two-photon profile. The main reason behind this assumption of redistribution is that the probability of coherent 1s–2s *scattering* event is tiny because the 2s–1s decay rate is extremely small compared to the time it takes to excite a 2s electron to higher levels or the continuum.

However, some additional simplifications are possible. First, we can again replace the factors, $(1+n)(1+n')$, accounting for stimulated two-photon emission with those from the undistorted CMB

blackbody. Furthermore, from equation (24),

$$n\,n' \approx \mathrm{e}^{-h\nu_{21}/kT_\gamma}\,(1+n^{\rm pl})(1+n^{\rm pl'})\left(1+\frac{\Delta n}{n^{\rm pl}}+\frac{\Delta n'}{n^{\rm pl'}}\right). \tag{28}$$

Also, since the spectral distortions at very low frequencies are never important, one of the two terms in equation (28) (say the one related to $\Delta n'$) can always be omitted. Therefore, we can rewrite equation (27) as

$$\frac{1}{c}\frac{\partial N_\nu}{\partial t}\bigg|^{\rm 2s1s}_{2\gamma} = A^{2\gamma}_{\rm 2s1s} N_{\rm 1s}\,\tilde{\varphi}^{2\gamma,*}_{\rm 2s}\left(\Delta n^{\rm 2s}_{\rm em} - f^{\rm 2s}_\nu \Delta n_\nu\right), \tag{29}$$

where $\tilde{\varphi}^{2\gamma,*}_{\rm 2s} \equiv \tilde{\varphi}^{2\gamma}_{\rm 2s}(1+n^{\rm pl})(1+n^{\rm pl'})$ and

$$\Delta n^{\rm 2s}_{\rm em} = \frac{X_{\rm 2s}}{X_{\rm 1s}} - \mathrm{e}^{-h\nu_{21}/kT_\gamma}, \tag{30a}$$

$$f^{\rm 2s}_\nu = \frac{\mathrm{e}^{-h\nu_{21}/kT_\gamma}}{n^{\rm pl}(\nu)} \approx \exp[h(\nu-\nu_{21})/kT_\gamma]. \tag{30b}$$

If the term $\frac{\Delta n'}{n^{\rm pl'}}$ is non-negligible, as might be the case at very low redshifts ($z \lesssim 400$), where the Lyman α photons emitted at $z \sim 1400$ redshifts into the 2s–1s absorption channel, one in addition has to subtract the term $f^{\rm 2s}_{\nu'}\Delta n_{\nu'}$ within the brackets of equation (29). In terms of $x = \nu/\nu_{21}$, z and Δn_x, the photon occupation number now evolves as

$$\frac{\partial \Delta n_x}{\partial z}\bigg|^{\rm 2s1s}_{2\gamma} = -\frac{\sigma^{2\gamma}_{\rm 2s1s} N_{\rm 1s} c}{H(1+z)}\,\frac{\phi^{2\gamma,*}_{\rm 2s}}{x^2}\left(\nu_{21}\,\Delta n^{\rm 2s}_{\rm em} - f^{\rm 2s}_x \Delta n_x\right). \tag{31}$$

Here, the 2s–1s cross-section is given by $\sigma^{2\gamma}_{\rm 2s1s} = \frac{\lambda^2_{21} A^{2\gamma}_{\rm 2s1s}}{8\pi\nu_{21}}$, and $\phi^{2\gamma,*}_{\rm 2s} = 4\,\pi\,\nu_{21}\tilde{\varphi}^{2\gamma,*}_{\rm 2s}$.

Equation (31) bears a striking resemblance to the emission and absorption in the Lyman-series channels as in equation (14) because one of the two photons that are involved in the 2s–1s two-photon process is drawn from the undistorted CMB blackbody spectrum, so that the evolution equation essentially becomes a *one-photon* equation. The difference is the absence of a death probability since practically every electron that is excited to the 2s state will take a detour to higher levels or the continuum as $p^{\rm 2s}_{\rm d} \approx 1$.

3.4 Two-photon emission and absorption terms from excited levels with $n > 2$

One of the most interesting modifications to the solution for the photon field is related to the deviations of the profiles for the different two-photon emission and absorption channels from the Lorentzian shape (Chluba & Sunyaev 2008). For the recombination problem, only those one-photon sequences involving a Lyman-series resonance (e.g. $4{\rm d} \leftrightarrow 2{\rm p} \leftrightarrow 1{\rm s}$) are important.[11] In this section, we shall replace the standard '1 + 1'-photon terms for these channels with the full two-photon description that takes into account the coherent nature of the process.[12]

[11] All the other two-photon emissions and absorption channels (e.g. $4{\rm d} \leftrightarrow 2{\rm p} \leftrightarrow 2{\rm s}$) can be treated within a blackbody ambient radiation field, so that their net rate can be directly computed. Without deviations from the blackbody shape, these will be extremely close to the normal '1 + 1'-photon rates. Also they can only affect the net recombination rate as a 'correction to correction', because they only act on the electron 'feeding rates' into the main channels towards the ground state. A similar argument holds for Raman-scattering events that do not directly connect to the ground state.

[12] Conditions persistent in the Universe at the recombination epoch make collisions negligible, maintaining the coherence of the two-photon decay (e.g. see Chluba & Sunyaev 2008; Hirata 2008)

We generalize the approach detailed in Chluba & Sunyaev (2010b) for emission of photons close to the Lyman α line to include corrections around the Lyman β and higher resonances.

3.4.1 Net rates for two-photon transitions from excited s and d states

The net change of the number density of electrons in the level $j \in \{n{\rm s}, n{\rm d}\}$ via the j-1s two-photon channel is given by

$$\begin{aligned}\frac{{\rm d}X_j}{{\rm d}t}\bigg|^{2\gamma}_{\rm 1s} &= \frac{g_j}{g_{\rm 1s}} A^{2\gamma}_{j\rm 1s} X_{\rm 1s}\int \varphi^{2\gamma}_j(\nu)\,n(\nu)\,n(\nu_{j1}-\nu)\,{\rm d}\nu \\ &\quad - A^{2\gamma}_{j\rm 1s} X_j \int \varphi^{2\gamma}_j(\nu)\,[1+n(\nu)][1+n(\nu_{j1}-\nu)]\,{\rm d}\nu.\end{aligned} \tag{32}$$

Here, $\varphi^{2\gamma}_j$ denotes the profile for the j-1s two-photon decay, which can be computed as explained in Appendix A, and is normalized[13] as $\int \varphi^{2\gamma}_j\,{\rm d}\nu = 1$. The (vacuum) two-photon decay rate is given by

$$A^{2\gamma}_{j\rm 1s} = \sum_{k=2}^{n_j-1} A_{j\,k\rm p}\,p^{k\rm p}_{\rm em}. \tag{33}$$

The ratio of the statistical weights is $g_j/g_{\rm 1s} = 1$ for the ns states, and $g_j/g_{\rm 1s} = 5$ for nd states. Equation (33) simply reflects the one-photon decay rates and branching ratios of all the '1 + 1'-photon routes $j \rightarrow n{\rm p} \rightarrow 1{\rm s}$ via intermediate p states with $n < n_j$. Stimulated emission induced by the CMB photons is not included in the definition of $A^{2\gamma}_{j\rm 1s}$, since it is taken into account differentially by the integrals in equation (32).

With notations defined in equation (21), and by following the procedure to derive equation (25), we can rewrite equation (32) as

$$\frac{{\rm d}X_j}{{\rm d}t}\bigg|^{2\gamma}_{\rm 1s} = A^{2\gamma,*}_{j\rm 1s}\left(\frac{g_j}{g_{\rm 1s}}\,X_{\rm 1s}\mathrm{e}^{-h\nu_{j\rm 1s}/kT_\gamma} - X_j\right) + \frac{g_j}{g_{\rm 1s}}\,A^{2\gamma}_{j\rm 1s}\,X_{\rm 1s}\,\Delta\mathcal{G}^j_1, \tag{34a}$$

$$\Delta\mathcal{G}^j_1 = 2\int_{\nu_{j\rm 1s}/2}^{\nu_{j\rm 1s}} \varphi^{2\gamma}_j\,n^{\rm pl'}\Delta n\,{\rm d}\nu, \tag{34b}$$

where we defined the stimulated j-1s two-photon decay rate within the CMB ambient radiation field as $A^{2\gamma,*}_{j\rm 1s} = A^{2\gamma}_{j\rm 1s}\,\mathcal{G}^{j,\rm pl}_2$.

The $\mathcal{G}^{j,\rm pl}_2$ depends crucially only on the CMB blackbody spectrum and thus can be pre-computed as a function of photon temperature, T_γ. On the other hand, like for the 2s–1s two-photon process (see equation 25), $\Delta\mathcal{G}^j_1$ arises due to *non-thermal* photons, and hence depends directly on the solution for the photon field.

In the normal '1 + 1'-photon picture, the two-photon profiles can be considered as a sum of δ-functions and therefore

$$A^{2\gamma(1+1),*}_{j\rm 1s} = \sum_{k=2}^{n_j-1} A^{*}_{j\,k\rm p}\,p^{k\rm p}_{\rm em}. \tag{35}$$

Here, $A^{*}_{j\rm kp} = A_{j\rm kp}\,[1+n^{\rm pl}(\nu_{jk})]$, and the stimulated effect close to the Lyman-series resonances has been neglected, i.e. $1+n^{\rm pl}(\nu_{k\rm p1s}) \approx 1$.

[13] Small corrections to the normalization due to the two-photon description are neglected.

3.4.2 Two-photon emission and absorption for excited s and d states

The two-photon emission and absorption terms are obtained by following the steps in the derivation of equation (31). For the j-1s two-photon channel, one therefore obtains

$$\left.\frac{\partial \Delta n_x}{\partial z}\right|_{2\gamma}^{j1s} = -\frac{\sigma_{j1s}^{2\gamma} N_{1s} c}{H(1+z)} \frac{\nu_{j1}^2}{\nu_{21}^2} \frac{\phi_j^{2\gamma,*}}{x^2} \left(\nu_{21}\, \Delta n_{\rm em}^j - f_x^j \Delta n_x\right). \quad (36)$$

The j-1s two-photon cross-section is given by $\sigma_{j1s}^{2\gamma} = \frac{g_j}{g_{1s}} \frac{\lambda_{j1}^2 A_{j1s}^{2\gamma}}{8\pi\nu_{j1}}$ and $\phi_j^{2\gamma,*} = 4\,\pi\,\nu_{j1}\tilde{\varphi}_j^{2\gamma}(\nu)\,[1+n^{\rm pl}(\nu)][1+n^{\rm pl}(\nu')]$, where, because of energy conservation, $\nu' = \nu_{j1s} - \nu$. Also,

$$\Delta n_{\rm em}^j = \frac{g_{1s}}{g_j}\frac{X_j}{X_{1s}} - {\rm e}^{-h\nu_{j1}/kT_\gamma}, \quad (37a)$$

$$f_\nu^j = \frac{{\rm e}^{-h\nu_{j1}/kT_\gamma}}{n^{\rm pl}(\nu)} \equiv \frac{{\rm e}^{h(\nu-\nu_{j1})/kT_\gamma}}{1+n^{\rm pl}(\nu)} \approx \exp\left[h(\nu-\nu_{j1})/kT_\gamma\right]. \quad (37b)$$

Again we emphasize the resemblance of the equation above to that of the one-photon equation for the Lyman-series emission and absorption channels as in equation (14).

3.4.3 Correcting the Lyman-series emission and absorption terms in the radiative transfer equation

Two-photon decays from a given initial state $j \in \{n{\rm s}, n{\rm d}\}$ involve Lyman-series resonances with $k < n$. For example, a 4d–1s two-photon emission event includes the effect of the Lyman α and β resonance. In the Lyman-series emission and absorption terms as in equation (14), these are already accounted for as '1 + 1'-photon terms, when the profile is given by the normal Voigt function.

To avoid the *double counting* of these transitions in the radiative transfer equation, two modifications are necessary: (i) all death probabilities, $p_{\rm d}^{k{\rm p}}$, have to be reduced to account only for those channels that are not included in the two-photon description and (ii) the Lyman-series emission rates have to be reduced for the same reason. This approach was also explained in Chluba & Sunyaev (2010b) for the 3s–1s and 3d–1s two-photon process. Including *only* the j-1s two-photon process (say for 3d–1s), the modified death probability and $\Delta\tilde{n}_{\rm em}^{k{\rm p}}$ of the Lyman-k resonance become

$$\tilde{p}_{\rm d}^{k{\rm p}} = p_{\rm d}^{k{\rm p}} - p_{\rm d}^{j,k{\rm p}}, \quad (38a)$$

$$\Delta\tilde{n}_{\rm em}^{k{\rm p}} = \frac{1}{3\,X_{1s}}\frac{R_{k{\rm p}}^{+} - R_{k{\rm p}}^{j,+}}{R_{k{\rm p}}^{-} - R_{k{\rm p}}^{j,-}} - {\rm e}^{-h\nu_{k{\rm p}}/kT_\gamma}, \quad (38b)$$

where the partial death probability, $p_{\rm d}^{j,k{\rm p}}$, is given by

$$p_{\rm d}^{j,k{\rm p}} = \frac{R_{k{\rm p}}^{j,-}}{A_{k{\rm p}1s} + R_{k{\rm p}}^{-}} \equiv p_{\rm em}^{k{\rm p}}\frac{R_{k{\rm p}}^{j,-}}{A_{k{\rm p}1s}} \equiv p_{\rm d}^{k{\rm p}}\frac{R_{k{\rm p}}^{j,-}}{R_{k{\rm p}}^{-}}. \quad (38c)$$

The partial rates in and out of the kp state are

$$R_{k{\rm p}}^{j,+} = A_{j\,k{\rm p}}[1+n^{\rm pl}(\nu_{j\,k{\rm p}})]\,X_j, \quad (38d)$$

$$R_{k{\rm p}}^{j,-} = \frac{g_j}{g_{k{\rm p}}}\,A_{j\,k{\rm p}}\,n^{\rm pl}(\nu_{j\,k{\rm p}}), \quad (38e)$$

such that $\frac{g_{1s}}{g_{k{\rm p}}}\frac{R_{k{\rm p}}^{j,+}}{R_{k{\rm p}}^{j,-}X_{1s}} \equiv n_{\rm L}^j\,{\rm e}^{h\nu_{j\,k{\rm p}}/kT_\gamma}$ with $n_{\rm L}^j = \frac{g_{1s}}{g_j}\frac{X_j}{X_{1s}}$.

When more than one two-photon channel is included, then for every Lyman resonance the following needs to be computed:

$$\tilde{p}_{\rm d}^{k{\rm p}} = p_{\rm d}^{k{\rm p}} - \sum_j p_{\rm d}^{j,k{\rm p}}, \quad (39a)$$

$$\Delta\tilde{n}_{\rm em}^{k{\rm p}} = \frac{1}{3\,X_{1s}}\frac{R_{k{\rm p}}^{+} - \sum_j R_{k{\rm p}}^{j,+}}{R_{k{\rm p}}^{-} - \sum_j R_{k{\rm p}}^{j,-}} - {\rm e}^{-h\nu_{k{\rm p}}/kT_\gamma}, \quad (39b)$$

where the sums run over all involved initial levels j.

3.4.4 Correcting the net rates in the multilevel atom

Equation (32) relates the population of level j with the ground state. The corresponding net two-photon transition rate includes the effect of all '1 + 1'-photon processes, $j \leftrightarrow n{\rm p} \leftrightarrow 1{\rm s}$, via Lyman-series resonances with $n < n_j$. Double-counting can again be avoided by subtracting the corresponding '1 + 1'-photon terms from the full j-1s two-photon rate. The remaining corrections can then be added to the effective multilevel code as additional rates which directly connects level j to the ground state.[14]

In the standard multilevel description of all $j \leftrightarrow n{\rm p} \leftrightarrow 1{\rm s}$ sequences ($n_j > n$), the contributions to the two-photon net rate as in equation (32) take the form (see also Chluba & Sunyaev 2010b)

$$\left.\frac{{\rm d}X_j}{{\rm d}t}\right|_{1{\rm s},k{\rm p}}^{2\gamma(1+1)} = \frac{g_{k{\rm p}}}{g_{1s}} X_{1s}\,A_{k{\rm p}1s}\,p_{\rm d}^{j,k{\rm p}}\,\bar{n}_{k{\rm p}1s} - X_j\,A_{j\,k{\rm p}}^{*}\,p_{\rm em}^{k{\rm p}}, \quad (40a)$$

$$\equiv \frac{g_j}{g_{1s}} X_{1s}\,A_{j\,k{\rm p}}\,p_{\rm em}^{k{\rm p}}\,n^{\rm pl}(\nu_{jk})\,\bar{n}_{k{\rm p}1s} - X_j\,A_{j\,k{\rm p}}^{*}\,p_{\rm em}^{k{\rm p}}, \quad (40b)$$

$$\left.\frac{{\rm d}X_j}{{\rm d}t}\right|_{1s}^{2\gamma(1+1)} = \sum_{k=2}^{n_j-1}\left.\frac{{\rm d}X_j}{{\rm d}t}\right|_{1{\rm s},k{\rm p}}^{2\gamma(1+1)}. \quad (40c)$$

Equation (40a) is interpreted as electrons exiting level j via the route $j \rightarrow n{\rm p} \rightarrow 1{\rm s}$ at a rate $A_{j\,k{\rm p}}^{*}$ times the probability, $p_{\rm em}^{k{\rm p}}$ (the second term). Similarly, electrons reach state j from the ground state via the route $1{\rm s} \rightarrow n{\rm p} \rightarrow j$, with the Lyman-$k$ excitation rate, $\frac{g_{k{\rm p}}}{g_{1s}}\,A_{k{\rm p}1s}\,\bar{n}_{k{\rm p}1s}$ times the probability, $p_{\rm d}^{j,k{\rm p}}$, to then make the transition $k{\rm p} \rightarrow j$ (the first term). Using equations (38c) and (38e) leads to equation (40b).

Equation (40b) helps make the connection of the full two-photon net rate and the '1 + 1'-photon terms because equation (40b) can be directly derived from equation (32), assuming that the two-photon profile is given by independent (non-interacting) resonances, where the line shapes are given by the normal Voigt profiles.

Substituting $\bar{n}_{k{\rm p}1s} = n^{\rm pl}(\nu_{k{\rm p}1s}) + \Delta\bar{n}_{k{\rm p}1s}$, and using the relation ${\rm e}^{h\nu/kT_\gamma} = [1+n^{\rm pl}(\nu)]/n^{\rm pl}(\nu)$, equation (40b) simplifies to

$$\left.\frac{{\rm d}X_j}{{\rm d}t}\right|_{1{\rm s},k{\rm p}}^{2\gamma(1+1)} = A_{j\,k{\rm p}}^{*}\,p_{\rm em}^{k{\rm p}}\left(\frac{g_j}{g_{1s}}X_{1s}\,{\rm e}^{-h\nu_{j1}/kT_\gamma} - X_j\right) + \frac{g_j}{g_{1s}}X_{1s}\,A_{j\,k{\rm p}}\,p_{\rm em}^{k{\rm p}}\,n^{\rm pl}(\nu_{j\,k{\rm p}})\,\Delta\bar{n}_{k{\rm p}1s}, \quad (41)$$

such that upon summing over the intermediate kp resonances, we have

$$\left.\frac{{\rm d}X_j}{{\rm d}t}\right|_{1s}^{2\gamma(1+1)} = A_{j1s}^{2\gamma(1+1),*}\left(\frac{g_j}{g_{1s}}X_{1s}\,{\rm e}^{-h\nu_{j1}/kT_\gamma} - X_j\right) + \frac{g_j}{g_{1s}}X_{1s}\sum_{k=2}^{k<n_j}A_{j\,k{\rm p}}\,p_{\rm em}^{k{\rm p}}\,n^{\rm pl}(\nu_{j\,k{\rm p}})\,\Delta\bar{n}_{k{\rm p}1s}. \quad (42)$$

[14] Chluba & Sunyaev (2010b) proposed a varied treatment in which the '1 + 1'-photon terms were first taken out of the standard network of rate equations and then the full two-photon rate between level j and 1s added, which at the end, is completely equivalent.

The above equation (34) reveals the correction term for the rate equations as

$$\Delta R^{2\gamma}_{j\leftrightarrow 1s} = A^{2\gamma}_{j1s}\,\Delta\mathcal{G}^j_2\left[\frac{g_j}{g_{1s}}\,X_{1s}\mathrm{e}^{-h\nu_{j1s}/kT_\gamma}-X_j\right] + A^{2\gamma}_{j1s}\,\frac{g_j}{g_{1s}}X_{1s}\left[\Delta\mathcal{G}^j_1-\sum_{k=2}^{k<n_j}\frac{A_{j\,kp}\,p^{kp}_{em}}{A^{2\gamma}_{j1s}}\,n^{pl}(\nu_{jkp})\,\Delta\bar{n}_{kp1s}\right]. \quad (43)$$

Here, we define $\Delta\mathcal{G}^j_2=\mathcal{G}^j_2-A^{2\gamma(1+1),*}_{j1s}/A^{2\gamma}_{j1s}$.

Similar to the 2s–1s two-photon channel, the correction to the rate equations here has two contributions. The first is related to $\Delta\mathcal{G}^j_2$, which is independent of the solution to the photon distribution and therefore can be pre-calculated, and the second arising from the integral $\Delta\mathcal{G}^j_1$. However, in contrast to the 2s–1s two-photon channel, in the normal rate equations, part of the latter term is already included. Thus, the '1 + 1'-photon term has to be subtracted (the last term in brackets), where this term is calculated using the Sobolev approximation for $\Delta\bar{n}_{kp1s}$.

$\Delta\mathcal{G}^j_2$, in principle, also arises in the normal '1 + 1' picture, when differentially accounting for the effect of stimulated emission in the CMB blackbody. However, the shape of the two-photon emission profile is crucial, since with the normal sum of Lorentzians the integrand in equation (21c) would diverge for $\nu\rightarrow\nu_{j1}$ and $\nu\rightarrow 0$ (Chluba & Sunyaev 2010b). Furthermore, the latter two terms in equation (43) account for both modifications in the shape of the full two-photon profiles and differences in the solution of the photon field in comparison with the standard Sobolev approximation.

The problem is numerical because two large terms are being subtracted. One way to achieve stable results is to split the range of integration into intervals where the mean occupation number in the standard Sobolev approximation is represented by (compare Chluba & Sunyaev 2009b)

$$\Delta\bar{n}_{kp1s} = \Delta n^{kp}_{L}\int_0^\infty\varphi^{kp}_V(\nu')\left[1-\mathrm{e}^{-\tau^{kp}_S(1-\chi^{kp}_{\nu'})}\right]\mathrm{d}\nu' = \Delta n^{kp}_{L}\left[\chi^{kp}_{\nu'}-\frac{\mathrm{e}^{-\tau^{kp}_S(1-\chi^{kp}_{\nu'})}}{\tau^{kp}_S}\right]_0^\infty=\Delta n^{kp}_{L}\left(1-P^{kp}_S\right), \quad (44)$$

with $\chi^{kp}_\nu=\int_0^\nu\varphi^{kp}_V\,\mathrm{d}\nu'$. Outside the resonances, one can simply compute each term in equation (43) separately, since there the contributions are small. For those intervals containing a resonance k on the other hand, one should compute both contributions in one integral, so that the main terms cancel. Clearly, the choice of the intervals is only motivated by the numerical precision that needs to be achieved. Since the Voigt profiles have their main support inside the Doppler core, it is sufficient to define regions of a few Doppler width around the resonances. This approach suffices for our purpose.

Alternatively, one can directly integrate the net two-photon production rate, equation (36), over frequency, and then subtract the net '1 + 1'-photon rate to obtain the correction. We confirmed that both approaches lead to the same answer.

To capture part of the dependence of $\Delta R^{2\gamma}_{j\leftrightarrow 1s}$ on the solution for the populations in numerical computations, we tabulate the function $\mathcal{F}^{2\gamma}_{j\leftrightarrow 1s}=\Delta R^{2\gamma}_{j\leftrightarrow 1s}/(X_{1s}\Delta n^j_L)$ as a function of redshift, once we computed the solution for the photon field using the results for the populations of the levels obtained from a run of our effective multilevel recombination code.

3.5 Raman scattering

In our previous work (Chluba & Sunyaev 2009a, 2010b), we did not consider the effect of the *Raman scattering* on the ionization history. However, the correction due to this process reaches $\Delta N_e/N_e\sim 0.9$ per cent at $z\sim 900$ (Hirata 2008), and hence demands careful consideration. The matrix element for this process is directly related to the one for the two-photon emission process by crossing-symmetry. In Appendix A, we explain how to compute the Raman-scattering profiles, $\varphi^R_j(\nu)$, for the j-1s Raman process. Additional details can also be found in Hirata (2008), where the importance of this effect during recombination was shown for the first time.

3.5.1 Net rates for ns–1s and nd–1s Raman scattering

The net change in the number density of electrons in the level $j\in\{n\mathrm{s},n\mathrm{d}\}$ caused by j-1s Raman scatterings is given by

$$\left.\frac{\mathrm{d}X_j}{\mathrm{d}t}\right|^R_{1s}=\frac{g_j}{g_{1s}}A^R_{j1s}X_{1s}\int_{\nu_{j1s}}^{\nu_{1sc}}\varphi^R_j(\nu-\nu_{j1s})\,n(\nu)\,[1+n(\nu-\nu_{j1s})]\,\mathrm{d}\nu - A^R_{j1s}X_j\int_0^{\nu_{jc}}\varphi^R_j(\nu)\,n(\nu)\,[1+n(\nu_{j1s}+\nu)]\,\mathrm{d}\nu, \quad (45a)$$

$$\equiv\frac{g_j}{g_{1s}}A^R_{j1s}X_{1s}\int_{\nu_{j1s}}^{\nu_{1sc}}\varphi^R_j(\nu-\nu_{j1s})\,n(\nu)\,[1+n(\nu-\nu_{j1s})]\,\mathrm{d}\nu - A^R_{j1s}X_j\int_{\nu_{j1s}}^{\nu_{1sc}}\varphi^R_j(\nu-\nu_{j1s})\,n(\nu-\nu_{j1s})\,[1+n(\nu)]\,\mathrm{d}\nu, \quad (45b)$$

where equation (45b) was simply obtained from equation (45a) by transforming the frequency range of the second integral.

In equation (45), φ^R_j denotes the j-1s Raman-scattering profile, and the Raman-scattering coefficient is given by[15]

$$A^R_{j1s}=\sum_{k=n_j+1}^{n_{max}}\frac{g_{kp}}{g_j}\,A_{kp\,j}\,p^{kp}_{em}. \quad (46)$$

The ratio of the statistical weights is $g_{kp}/g_j=3$ for the ns states, and $g_{kp}/g_j=3/5$ for nd states. Equation (46) simply reflects the one-photon terms and branching ratios of all the '1 + 1'-photon routes $j\rightarrow n\mathrm{p}\rightarrow 1\mathrm{s}$ via intermediate p states with $n>n_j$.

A rigorous treatment of equation (46) would include the integral over continuum states. However, any electron reaching the continuum would forget its history because of fast Coulomb interactions resulting in decoherence of the Raman process in the continuum. Furthermore, as mentioned above, the Lyman continuum is extremely optically thick such that these channels will always cancel out (see also Hirata 2008). Also, in numerical computations we only follow the evolution of the photon field up to some maximal frequency, ν_{max}. Therefore, in our description, we are not accounting for the full Raman process connected with transitions involving photons with $\nu>\nu_{max}$. This approximation is fully justified as the higher Lyman series contribute negligible amounts to the total recombination rate. Thus, the sum over intermediate p states become finite without significant loss of precision.

To simplify equation (45), we define the following quantities:[16]

$$\langle\,f(\nu)\,\rangle^R_i=\int_{\nu_{i1s}}^{\nu_{max}}\varphi^R_i(\nu-\nu_{j1s})\,f(\nu)\,\mathrm{d}\nu, \quad (47a)$$

[15] We call A^R_{j1s} 'coefficient' since in vacuum there is no Raman process.

[16] Formally, the upper limit of the integral over the Raman profiles should go to infinity. However, since we are following the spectrum in a finite range of frequencies, this introduces an upper limit, $\nu_{max}\leq\nu_{1sc}$.

$$\mathcal{R}_1^i = \langle\, n\,(1+n')\,\rangle_i^{\rm R}, \tag{47b}$$

$$\mathcal{R}_2^i = \langle\, n'(1+n)\,\rangle_i^{\rm R}, \tag{47c}$$

with $n' = n(\nu - \nu_{j1s})$. In the spirit of the two-photon emission and absorption process, we can now write

$$\begin{aligned}\mathcal{R}_1^i &\approx \langle\, n^{\rm pl}\,(1+n^{\rm pl'})\,\rangle_i^{\rm R} + \langle\, \Delta n\,(1+n^{\rm pl'})\,\rangle_i^{\rm R} \\ &\approx \mathcal{R}_2^i\, {\rm e}^{-h\nu_{j1s}/kT_\gamma} + \langle\, \Delta n\,(1+n^{\rm pl'})\,\rangle_i^{\rm R}\end{aligned} \tag{48a}$$

$$\mathcal{R}_2^i \approx \langle\, n^{\rm pl'}(1+n^{\rm pl})\,\rangle_i^{\rm R} = A^{\rm R,*}_{j1s}/A^{\rm R}_{j1s}. \tag{48b}$$

The total $j \rightarrow$ 1s '1 + 1' Raman-scattering rate in the CMB blackbody ambient radiation field is

$$A^{\rm R(1+1),*}_{j1s} = \sum_{k=n_j+1}^{n_{\rm max}} \frac{g_{k\rm p}}{g_j} A_{k\rm p\,j}\, n^{\rm pl}(\nu_{jk})\, p^{k\rm p}_{\rm em}. \tag{49}$$

This then leads to

$$\left.\frac{{\rm d}N_j}{{\rm d}t}\right|_{1s}^{\rm R} = A^{\rm R,*}_{j1s}\left(\frac{g_j}{g_{1s}}\, X_{1s}{\rm e}^{-h\nu_{j1s}/kT_\gamma} - X_j\right) + \frac{g_j}{g_{1s}}\, A^{\rm R}_{j1s}\, X_{1s}\, \Delta\mathcal{R}_1^j, \tag{50a}$$

$$\Delta\mathcal{R}_1^j = \int_{\nu_{j1s}}^{\nu_{\rm max}} \varphi_j^{\rm R}(\nu - \nu_{j1s})\,(1+n^{\rm pl'})\,\Delta n(\nu)\,{\rm d}\nu. \tag{50b}$$

Here $A^{\rm R,*}_{j1s}$ and $\Delta\mathcal{R}_1^j$ are important in defining the correction to the rate equations (see Section 3.5.4). Again $A^{\rm R,*}_{j1s}$ is the thermal contribution, while $\Delta\mathcal{R}_1^j$ arises from non-thermal photons.

3.5.2 Terms in the radiative transfer equation for the Raman scattering

From equation (45), the terms in the radiative transfer equation for the photon field can be obtained. However, one aspect is important to keep in mind: a photon that Raman scatters off an electron in the jth state is removed from frequencies $0 \le \nu \le \nu_{jc}$. However, the scattered photon appears in the frequency range $\nu_{jc} < \nu_{j1} \le \nu' \le \nu_{1c}$, and likewise for the inverse process. This description assumes *complete redistribution* of photons over the full Raman-scattering profile[17] during each scattering event. Therefore, the terms for the radiative transfer equation read as follows:

$$\begin{aligned}\frac{1}{c}\left.\frac{\partial N_\nu}{\partial t}\right|_{{\rm R},\nu\le\nu_{jc}}^{j1s} &= \frac{g_j}{g_{1s}} A^{\rm R}_{j1s} N_{1s}\, \tilde{\varphi}_j^{\rm R}(\nu)\, n(\nu_{j1s}+\nu)\,[1+n(\nu)] \\ &\quad - A^{\rm R}_{j1s} N_j\, \tilde{\varphi}_j^{\rm R}(\nu)\, n(\nu)\,[1+n(\nu_{j1s}+\nu)],\end{aligned} \tag{51a}$$

$$\begin{aligned}\frac{1}{c}\left.\frac{\partial N_\nu}{\partial t}\right|_{{\rm R},\nu_{j1s}\le\nu}^{j1s} &= A^{\rm R}_{j1s} N_j\, \tilde{\varphi}_j^{\rm R}(\nu-\nu_{j1s})\, n(\nu-\nu_{j1s})\,[1+n(\nu)] \\ &\quad - \frac{g_j}{g_{1s}} A^{\rm R}_{j1s} N_{1s}\, \tilde{\varphi}_j^{\rm R}(\nu-\nu_{j1s})\, n(\nu)\,[1+n(\nu-\nu_{j1s})],\end{aligned} \tag{51b}$$

where $\tilde{\varphi}_j^{\rm R}(\nu) = \varphi_j^{\rm R}(\nu)/4\pi$. It is clear that the total integral over frequency vanishes, when adding the above two terms, showing that the Raman process conserves photon number. However, the number density of electrons in the 1s and j state is altered after each Raman-scattering event, according to equation (45).

[17] We neglect corrections caused by partial redistribution in the Raman-scattering events, but like in the case of two-photon transitions these should be very small.

With regards to the recombination dynamics, we are not interested in the changes to the photon spectrum at low frequencies. Therefore, we only consider equation (51b). For stimulated terms, the distortions can be neglected. Furthermore, one can define $\tilde{\varphi}_j^{\rm R,*}(\nu) \equiv \tilde{\varphi}_j^{\rm R}(\nu)\, n^{\rm pl}(\nu)\,[1+n^{\rm pl}(\nu_{j1s}+\nu)] \approx \tilde{\varphi}_j^{\rm R}(\nu)\, n^{\rm pl}(\nu)$, and neglect the distortions at low frequencies, such that

$$\begin{aligned}\frac{1}{c}\left.\frac{\partial N_\nu}{\partial t}\right|_{{\rm R},\nu_{j1s}\le\nu}^{j1s} &\approx A^{\rm R}_{j1s} N_j\, \tilde{\varphi}_j^{\rm R,*}(\nu-\nu_{j1s}) \\ &\quad - \frac{g_j}{g_{1s}} A^{\rm R}_{j1s} N_{1s}\, \tilde{\varphi}_j^{\rm R,*}(\nu-\nu_{j1s})\, f_\nu^j\, n(\nu),\end{aligned} \tag{52}$$

where f_ν^j is defined by equation (37b). In terms of the photon occupation number, this equation becomes

$$\left.\frac{\partial \Delta n_x}{\partial z}\right|_{{\rm R},\nu_{j1s}\le\nu}^{j1s} = -\frac{\sigma^{\rm R}_{j1s} N_{1s} c}{H[1+z]}\, \frac{\nu_{j1}^2}{\nu_{21}^2}\, \frac{\phi_j^{\rm R,*}}{x^2}\left(\nu_{21}\,\Delta n^j_{\rm em} - f_x^j \Delta n_x\right), \tag{53}$$

where $\Delta n^j_{\rm em}$ is defined as in equation (37a). The j-1s Raman-scattering cross-section is given by $\sigma^{\rm R}_{j1s} = \frac{g_j}{g_{1s}}\, \frac{\lambda_{j1}^2 A^{\rm R}_{j1s}}{8\pi\nu_{j1}}$, and we set $\phi_j^{\rm R,*} \equiv 4\,\pi\,\nu_{j1}\tilde{\varphi}_j^{\rm R,*}(\nu-\nu_{j1s})$. Note the close similarity of this equation to the one-photon equation for the Lyman-series emission and absorption channels in equation (14). Photons scattering from frequencies $0 \le \nu \le \nu_{jc}$ into the range $\nu_{j1s} \le \nu$ appear as a source term. This is related to the fact that these photons are drawn from the CMB blackbody.

3.5.3 Correcting the Lyman-series emission and absorption terms in the radiative transfer equation

Like in the case of two-photon emission and absorption, the resonant part of the Raman process is already part of the '1 + 1'-photon Lyman-series transfer in equation (14). To avoid double counting, we simply have to correct the death probability and $\Delta n^{k\rm p}_{\rm em}$ of the Lyman-k resonance for terms that are included in the Raman-scattering process. For example, when using the terms for the 2s–1s Raman-scattering process in the radiative transfer equation, $p_{\rm d}^{k\rm p}$ and $\Delta n^{k\rm p}_{\rm em}$ for Lyman β, γ, δ and higher will have to be corrected.

The modified death probability can be obtained by adding appropriate terms to the sums of equation (39). However, for each included Raman channels one now has $R^{j,-}_{k\rm p} = A_{k\rm p\,j}\,[1+n^{\rm pl}(\nu_{j\,k\rm p})]$, and $R^{j,+}_{k\rm p} = \frac{g_{k\rm p}}{g_j}\, A_{k\rm p\,j}\, n^{\rm pl}(\nu_{j\,k\rm p})\, X_j \equiv R^{j,-}_{k\rm p}\, \frac{g_{k\rm p}}{g_j}\, X_j\, {\rm e}^{-h\nu_{j\,k\rm p}/kT_\gamma}$.

3.5.4 Correcting the net rates in the multilevel atom

Like in the case of two-photon emission and absorption events, corrections to the net rates in the multilevel atom have to be defined to avoid double counting. In the standard multilevel description of all $j \leftrightarrow n{\rm p} \leftrightarrow 1{\rm s}$ sequences ($n_j < n$), the contributions to the Raman-scattering net rate, equation (45), take the following form:

$$\left.\frac{{\rm d}X_j}{{\rm d}t}\right|_{1s,k\rm p}^{\rm R(1+1)} = \frac{g_{k\rm p}}{g_{1s}} X_{1s}\, A_{k\rm p1s}\, p_{\rm d}^{j,k\rm p}\, \bar{n}_{k\rm p1s} - \frac{g_{k\rm p}}{g_j} X_j\, A_{k\rm p j}\, n^{\rm pl}(\nu_{jk}) p^{k\rm p}_{\rm em}, \tag{54a}$$

$$\equiv \frac{g_{k\rm p}}{g_{1s}} X_{1s}\, A^*_{k\rm p j}\, p^{k\rm p}_{\rm em}\, \bar{n}_{k\rm p1s} - \frac{g_{k\rm p}}{g_j} X_j\, A_{k\rm p j}\, n^{\rm pl}(\nu_{jk}) p^{k\rm p}_{\rm em}, \tag{54b}$$

$$\left.\frac{{\rm d}X_j}{{\rm d}t}\right|_{1s}^{\rm R(1+1)} = \sum_{k=n_j+1}^{n_{\rm max}} \left.\frac{{\rm d}X_j}{{\rm d}t}\right|_{1s,k\rm p}^{\rm R(1+1)}. \tag{54c}$$

As mentioned above, $n_{\rm max}$ is a consequence of the finite computational domain. The terms in equation (54) are interpreted as in the case of two-photon emission and absorption (see Section 3.4.4).

Inserting $\bar{n}_{k\rm p1s} = n^{\rm pl}(\nu_{k\rm p1s}) + \Delta\bar{n}_{k\rm p1s}$ and using the relation $\mathrm{e}^{h\nu/kT_\gamma} = [1 + n^{\rm pl}(\nu)]/n^{\rm pl}(\nu)$, equation (54b) simplifies to

$$\left.\frac{\mathrm{d}X_j}{\mathrm{d}t}\right|^{\rm R(1+1)}_{\rm 1s,k\rm p} = \frac{g_{k\rm p}}{g_j} A_{k\rm p\,\it j}\, n^{\rm pl}(\nu_{j k}) p^{k\rm p}_{\rm em} \left(\frac{g_j}{g_{\rm 1s}} X_{\rm 1s}\, \mathrm{e}^{-h\nu_{j1}/kT_\gamma} - X_j\right) + \frac{g_{k\rm p}}{g_{\rm 1s}} X_{\rm 1s}\, A^{*}_{k\rm p\,\it j}\, p^{k\rm p}_{\rm em}\, \Delta\bar{n}_{k\rm p1s}, \quad (55)$$

such that summing over the intermediate kp resonances leads to

$$\left.\frac{\mathrm{d}X_j}{\mathrm{d}t}\right|^{\rm R(1+1)}_{\rm 1s} = A^{\rm R,*}_{j1\rm s}\left(\frac{g_j}{g_{\rm 1s}} X_{\rm 1s}\, \mathrm{e}^{-h\nu_{j1}/kT_\gamma} - X_j\right) + X_{\rm 1s} \sum_{k=n_j+1}^{n_{\rm max}} \frac{g_{k\rm p}}{g_{\rm 1s}}\, A^{*}_{k\rm p\,\it j}\, p^{k\rm p}_{\rm em}\, \Delta\bar{n}_{k\rm p1s}. \quad (56)$$

Using equation (50), it is clear that the correction term for the rate equations is

$$\Delta R^{\rm R}_{j\leftrightarrow 1\rm s} = A^{\rm R}_{j1\rm s}\, \Delta\mathcal{R}^j_2 \left(\frac{g_j}{g_{\rm 1s}}\, X_{\rm 1s}\mathrm{e}^{-h\nu_{j1\rm s}/kT_\gamma} - X_j\right) + A^{\rm R}_{j1\rm s}\, \frac{g_j}{g_{\rm 1s}} X_{\rm 1s} \left(\Delta\mathcal{R}^j_1 - \sum_{k=n_j+1}^{n_{\rm max}} \frac{g_{k\rm p}}{g_j}\, \frac{A^{*}_{k\rm p\,\it j}\, p^{k\rm p}_{\rm em}}{A^{\rm R}_{j1\rm s}}\, \Delta\bar{n}_{k\rm p1s}\right), \quad (57)$$

where we define $\Delta\mathcal{R}^j_2 = \mathcal{R}^j_2 - A^{\rm R(1+1),*}_{j1\rm s}/A^{\rm R}_{j1\rm s}$. Like for the two-photon channels (see equation 43), $\Delta\mathcal{R}^j_2$, in principle, also arises in the normal '1 + 1' picture, where the shape of the Raman profile ensures that the integrand remains finite, this time in the limit of $\nu \rightarrow \nu_{j1\rm s}$ (see Appendix A2). Furthermore, the latter two terms in equation (57) account for both modifications in the shape of the Raman profiles with respect to the normal sum of Lorentzians and differences in the solution of the photon field with respect to the Sobolev approximation.

Again one can compute the integrals over frequency by splitting the range of integration and using equation (44) to model the 'Sobolev part'. In numerical calculations, we tabulate $\mathcal{F}^{\rm R}_{j\leftrightarrow 1\rm s} = \Delta R^{\rm R}_{j\leftrightarrow 1\rm s}/(X_{\rm 1s}\, \Delta n^j_{\rm L})$ versus redshift to include the correction into the effective multilevel recombination code, and then use this to correct the rate equations.

4 CHANGES IN THE LYMAN-SERIES DISTORTION FOR DIFFERENT PHYSICAL PROCESSES

In Section 5, we discuss the changes to the free electron fraction due to the various physical processes under consideration. However, in order to understand the source of these corrections, it is illustrative to first look at the modifications in the Lyman-series spectral distortion.

In Fig. 1, we present the spectral distortion at two different redshifts, one before the maximum of the Lyman-series emission (which happens at $z \sim 1300$–1400), and one just before the maximum of the Thomson visibility function. We include Lyman resonances up to $n = 8$ for these computations. The solutions to the populations of the hydrogen levels were obtained from our implementation of the effective 400-shell recombination code.

The solid black line in all the panels shows our *reference case*, for which the Lyman series is modelled using Voigt profiles. This case already includes the effect of *resonance scattering* (for all Lyman-series resonances), *electron scattering*, the full *time-dependence* (Chluba & Sunyaev 2009b) of the emission and absorption process, and the *thermodynamic correction* factor for each resonance (Chluba & Sunyaev 2010b), capturing a large part of the corrections with respect to the Sobolev treatment. In particular, the distinction between scattering and emission/absorption events (by introducing the death probability) is important for the photon distribution on the blue side of the Lyman α resonance (see discussion in Chluba & Sunyaev 2009b). Furthermore, time-dependence and the thermodynamic correction factor lead to a large modification of the photon distribution with respect to the standard Sobolev case.

We will now discuss the effect of the different processes on the shape of the Lyman-series distortion separately.

4.1 Effect of Lyman-series scattering

In Fig. 1, the dotted curve shows the case for which we 'switched off' the terms for Lyman-series scattering. This line is only visible in the upper panels, since at high frequencies above the Lyman α line it coincides with the reference case. The figure illustrates that partial redistribution by Lyman-series scattering is only important close to the Lyman α resonance, and on its red wing. We could, in principle, neglect the correction due to resonance scattering for Lyman n with $n > 2$; however, with our efficient PDE solver, it is straightforward to take them into account.

The physical reason for this behaviour is that the scattering probability in the Lyman α line is very close to unity ($p^{2\rm p}_{\rm sc} \sim 0.999$–$0.9999$), such that only in the vicinity of the Doppler core can real emission and absorption terms act efficiently, strongly redistributing photons over frequency. Outside the Doppler core, however, redistribution is much slower making the effect of Doppler redistribution visible.

For the higher Lyman-series resonance, on the other hand, the death probability is only about an order of magnitude smaller than the scattering probability, implying that far out in the wings of the resonance photons can be efficiently redistributed by emission and absorption processes. In this case, resonance scattering leads to a small correction (see also arguments in Ali-Haïmoud et al. 2010).

4.2 Two-photon emission and absorption from the excited states with $n \geq 3$

Next we include the corrections due to the *shapes* of the ns–1s and nd–1s two-photon profiles (Fig. 1, red/dashed line). By *shape*, we also address modifications caused by the presence of CMB blackbody photons.

One can see that in comparison to the reference case, this slightly decreases the spectral distortion between all Lyman resonances, indicating that the emission/absorption opacity has decreased. The largest effect is seen between the Lyman α and Lyman β lines, as a result of the 3s–1s and 3d–1s two-photon emission and absorption process. This result is in agreement with our earlier treatment (Chluba & Sunyaev 2010b), where it was demonstrated that the shape of the 3s–1s and 3d–1s two-photon profiles leads to a slight acceleration of recombination, which, however, is less important than the corrections arising from the thermodynamic correction factor and time-dependence, individually.

We tried to identify the main source of the modifications above the Lyman β resonance in more detail. In the full two-photon picture, the 3s–1s and 3d–1s two-photon emission and absorption channels only act on photons with $\nu \leq \nu_{31}$. However, when neglecting the

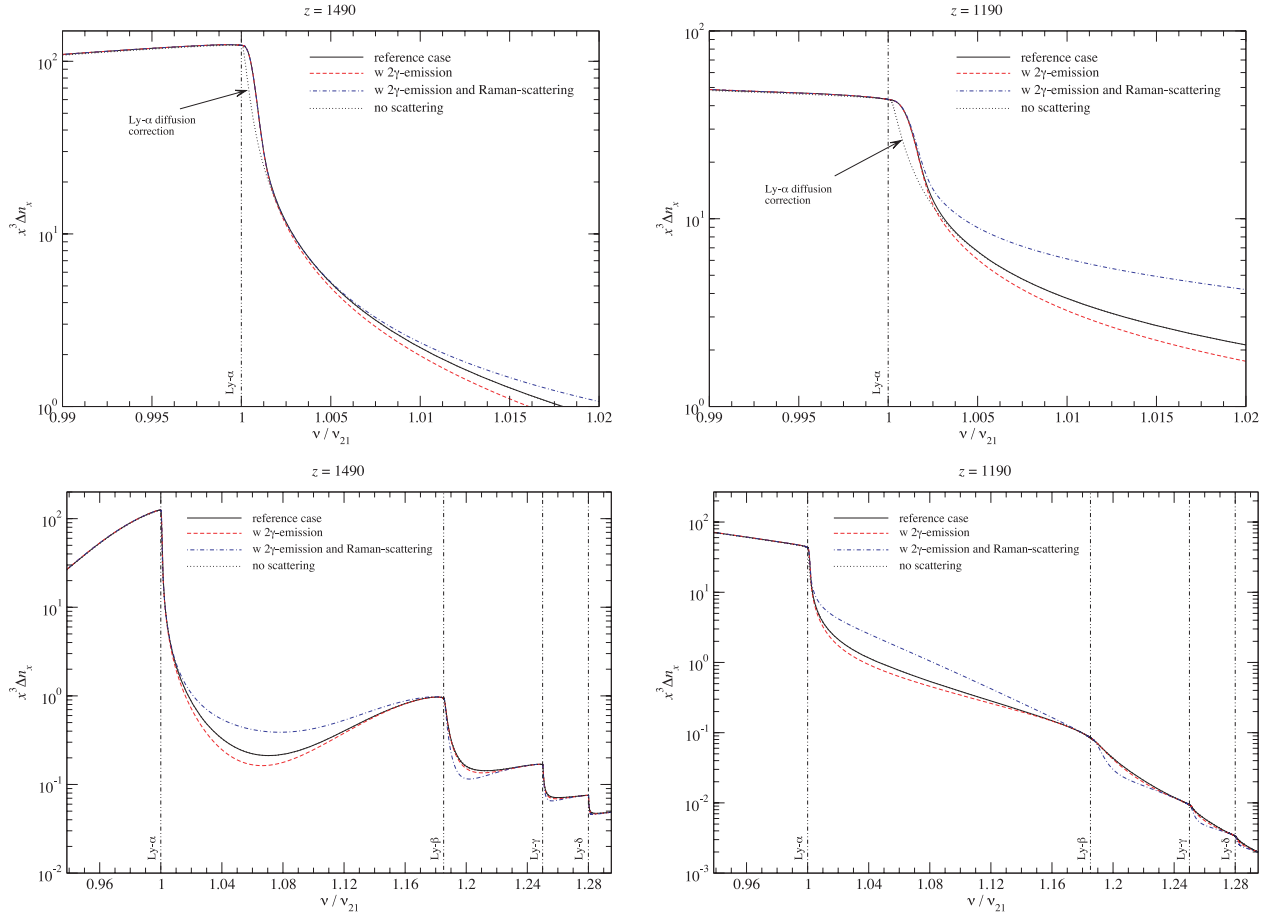

Figure 1. Solution for the Lyman-series distortion at $z = 1490$ (left-hand panels) and $z = 1190$ (right-hand panels) for different combinations of physical processes (for details see Section 4). In all the cases, we include the effect of electron scattering. We also marked the positions of the Lyman-series resonances with the vertical dashed-dot-dotted lines. The effect of partial frequency redistribution is only important close to the Lyman α line centre, so that the dotted line is only visible in the upper panels. A movie on the time-evolution of the Lyman-series distortion can be found at www.Chluba.de/Lyman-series-movie.

modifications to the shapes of the two-photon profiles, a large part of the opacity above the Lyman β line (incorrectly) comes from the 3s–1s and 3d–1s '$1 + 1$'-photon channel, which involves the Lyman α resonance and is modelled by a normal Voigt profile. It turns out that only for the 3s–1s and 3d–1s two-photon process does the exact shape of the two-photon profile really matter. Above the Lyman β line, the small correction with respect to the solid line is practically captured by *truncating* the Voigt profiles (in particular the one for Lyman α), such that the energy is conserved (e.g. photons emitted or absorbed in a 3s–1s and 3d–1s '$1 + 1$'-photon process can only have energies $\nu \leq \nu_{31}$, and so on). This illustrates how important the shape of the line profiles is when going far into the damping wings of the resonances.

4.3 Importance of Raman scattering

In addition to the two-photon corrections, we ran cases that also include the full Raman-scattering treatment (Fig. 1, blue/dash–dotted line). One can see that the Raman process led to an enhancement of the spectral distortion between the Lyman α and Lyman β resonance, while in all the other cases the spectral distortion decreases between the resonances. Thus, one expects an increased blue-wing feedback correction and hence a delay of hydrogen recombination from Lyman α. On the other hand, these additional red-wing Lyman β photons were created in a 2s–1s Raman event, such that at earlier times an acceleration is expected. This simple picture is in agreement with earlier discussions of this process (Hirata 2008).

In the case considered, the main source of the difference in the Lyman-series distortion comes from the 2s–1s Raman treatment. Neglecting the Raman corrections to the higher ns–1s and nd–1s channels does no affect the shape of the distortion notably. This is one of the reasons why the Raman process need to be included only for the first few levels.

Since in the case of Raman scattering, the 2s $\rightarrow$ 1s scattering profile is given by $\tilde{\varphi}_j^{\mathrm{R},*}(\nu) \approx \tilde{\varphi}_j^{\mathrm{R}}(\nu)\, n^{\mathrm{pl}}(\nu)$ (see Section 3.5), one expects two sources of corrections: (i) due to the difference of $\varphi_j^{\mathrm{R}}(\nu)$ with respect to a sum of Voigt profiles with appropriate weights and (ii) the factor of $n^{\mathrm{pl}}(\nu)$. In the normal '$1 + 1$'-photon picture, this factor would not appear differentially, but instead directly for each resonance frequency. It turns out that both parts of the correction are important for the 2s–1s Raman treatment.

We note that the spectral distortion at $z = 1190$ in the full treatment looks very similar to the curve given in Hirata (2008). However, in Hirata (2008) also the CMB blackbody spectrum was added, and n_ν instead of $x^3 \Delta n_x$ was plotted, which makes a direct comparison more difficult.

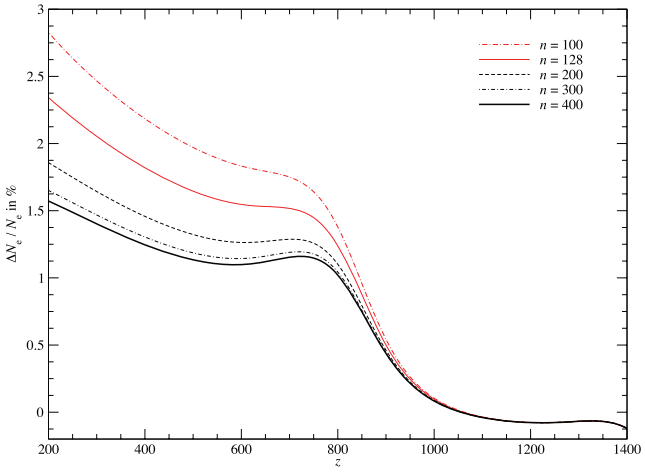

Figure 2. Dependence of the modifications to the recombination dynamics on the number of included shells. The results of our effective multilevel recombination code were directly compared with the output from RECFAST.

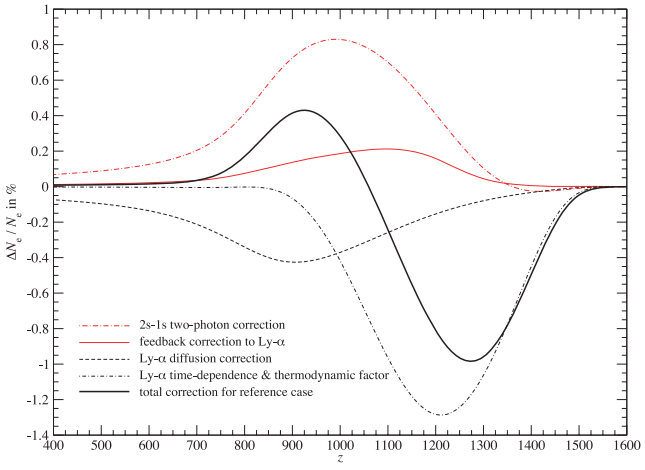

Figure 3. Corrections that are included into the reference case.

5 CHANGES TO THE FREE ELECTRON FRACTION FOR DIFFERENT PHYSICAL PROCESSES

In this section, we present our analysis of the different corrections to the standard recombination calculation. We focus on hydrogen, and model the helium recombination dynamics using the description given in Chluba & Sunyaev (2010a), including the first five shells with full feedback. With the current version of our effective multilevel recombination code, we are able to account for all important corrections to the recombination dynamics of hydrogen. We show a direct comparison with previous results and find very good agreement. All figures in which we compared the output of our recombination code with RECFAST we used RECFAST v1.4.2 (Wong & Scott 2007), but excluded the corrections to the helium recombination history in RECFAST and removed the switches in the RECFAST ordinary differential equation (ODE) system (see Fendt et al. 2009, for details). The cumulative effect on the ionization history is presented in Fig. 6.

5.1 Results from our effective multilevel code

In Fig. 2, we show the changes in the recombination dynamics with the number of shells that were included into the computation of the effective rates. This figure confirms that our implementation of the effective multilevel approach yields corrections that are in agreement with our earlier computations Chluba et al. (2010). We find that the correction converges down to $z \sim 200$ when including $\sim$300–400 shells as already explained in Chluba et al. (2010). We also directly compared with our full multilevel recombination code and found the difference to be smaller than $\Delta N_{\rm e}/N_{\rm e} \sim 10^{-5}$.

Collisional processes are still able to change the low-redshift behaviour at the $\sim$0.1 per cent level in this redshift range (Chluba et al. 2010), however, we defer a detailed analysis on the importance of this effect to a future work.

5.2 The reference case

In Fig. 3, we present a compilation of different corrections to the ionization history that are included into our reference case. For this, we *internally* compared the outputs of our recombination code when switching on and off different processes. We computed the solution to the photon transfer problem including the Lyman series up to $n = 8$ with Lyman θ ($n = 9$) on the upper boundary of the frequency grid. In the Lyman-series transfer, we did not include the corrections to the *profiles* of the emission and absorption processes arising from two-photon and Raman events, i.e. we described Lyman-k emission and absorption using equation (14). However, in our full reference case, Lyman-k resonance and electron scattering, as well as 2s–1s two-photon emission and absorption were included (see Section 4 for additional comments).

To account for all the corrections to the rate equations in the effective multilevel recombination code, we ran the obtained solution for the photon distribution through the modules that also allow us to take the two-photon and Raman-scattering corrections into account (see explanations in Section 3). However, we replaced the full profiles of the channels with the normal Voigt profiles.

The cumulative difference with respect to the output of our effective multilevel recombination code which does not include any of the radiative transfer corrections is shown in Fig. 3. In total, we find a delay in recombination by $\Delta N_{\rm e}/N_{\rm e} \sim 0.4$ per cent at $z \sim 930$, and an early acceleration by $\Delta N_{\rm e}/N_{\rm e} \sim -1.0$ per cent at $z \sim 1270$. The reference case, therefore, captures a significant part of the total correction with respect to RECFAST (see Section 5.5 for details).

5.2.1 *The 2s–1s two-photon correction*

Fig. 3 shows the total correction due to changes in the 2s–1s two-photon channel. We only modified the 2s–1s two-photon and Lyman α net rate in our effective multilevel recombination code using equation (26), but did not alter any of the other rates. Also we switched off line diffusion.

We find a delay of recombination by $\Delta N_{\rm e}/N_{\rm e} \sim 0.83$ per cent at $z \sim 990$, which is slightly (by $\Delta N_{\rm e}/N_{\rm e} \sim 0.18$ per cent) larger than in earlier computations of this process (e.g. Fendt et al. 2009).

There are two main reasons for this difference: (i) because in the reference case we include the emission and absorption in the 2s–1s two-photon channel, the *self-feedback* of photons emitted by 2s–1s transitions on the 1s–2s two-photon channel is accounted for, which leads to an additional delay of $\Delta N_{\rm e}/N_{\rm e} \sim 0.08$ per cent and (ii) the remaining deceleration by $\Delta N_{\rm e}/N_{\rm e} \sim 0.1$ per cent is just caused by normal absorption of 2s–1s photons by Lyman α (without the aid of line diffusion).

5.2.2 Feedback to Lyman α and the diffusion correction

We now considered the feedback correction to Lyman α. Like in our earlier treatment (Chluba & Sunyaev 2007), we find $\Delta N_{\rm e}/N_{\rm e} \sim 0.21$ per cent at $z \sim 1100$. We computed this correction from our radiative transfer code by modifying the Lyman α escape probability, with resonance scattering switched off. We also left the rate equations for the higher Lyman-series resonances unaffected, in order to not reflect the full Lyman-series feedback correction, which amounts to $\Delta N_{\rm e}/N_{\rm e} \sim 0.26$ per cent at $z \sim 1100$ (Chluba & Sunyaev 2010a).

In Fig. 3, the correction due to Lyman α diffusion alone is depicted. Again this was computed as a correction to the Lyman α resonance only. We find an acceleration by $\Delta N_{\rm e}/N_{\rm e} \sim -0.44$ per cent at $z \sim 900$. This is slightly smaller than in our earlier computation (Chluba & Sunyaev 2009a). The reason is simply that there we included only three shells into our computation. However, when including more than 5–10 shells the diffusion correction becomes slightly smaller, reducing to the curve presented in Fig. 3. To check the precision of our PDE solver, we recomputed the curve for the three-shells case and confirmed our earlier result.

5.2.3 The correction due to time-dependence and thermodynamic factor

The final correction that is taken into account by the computations in the reference case is caused by the time-dependence of the Lyman α emission process and the thermodynamic correction factor (see Fig. 3). The origin of these terms was first explained in detail by Chluba & Sunyaev (2009b) and Chluba & Sunyaev (2010b). The net effect is an acceleration in recombination by $\Delta N_{\rm e}/N_{\rm e} \sim -1.28$ per cent at $z \sim 1200$. This result is in excellent agreement with the curves presented in Chluba & Sunyaev (2010b), fig. 18 therein. Note that also in the figure of Chluba & Sunyaev (2010b), the 3s–1s and 3d–1s two-photon profile correction was included.

5.2.4 Correction from the higher Lyman n

For the solid black line in Fig. 3, all Lyman-series corrections were included. However, so far we have just discussed the corrections to the 2s–1s two-photon and Lyman α channel. We found a cumulative acceleration by $\Delta N_{\rm e}/N_{\rm e} \sim -0.06$ per cent at $z \sim 1210$ as result of the higher Lyman series. This correction includes all feedback corrections among the higher levels, time-dependence and the thermodynamic factors. Since the additional modification is small, this shows that just a detailed treatment of 2s–1s two-photon and Lyman α corrections already gives a very good approximation to the total correction in the reference case.

5.3 Two-photon corrections from levels with $n > 2$

In this section, we discuss the correction caused by the modifications in the emission and absorption profiles of the ns–1s and nd–1s two-photon channels. These corrections are due to (i) *quantum-mechanical* modifications to the shapes of the line profiles and (ii) *stimulated* two-photon emission in the CMB blackbody radiation field. For two-photon processes from ns and nd states with $n > 2$, the former dominates.

In Fig. 4, we present the changes to the free electron fraction when the two-photon corrections up to the 8s–1s and 8d–1s two-photon channel are included. Two-photon processes lead to a total acceleration of recombination by $\Delta N_{\rm e}/N_{\rm e} \sim -0.46$ per cent at $z \sim 1120$.

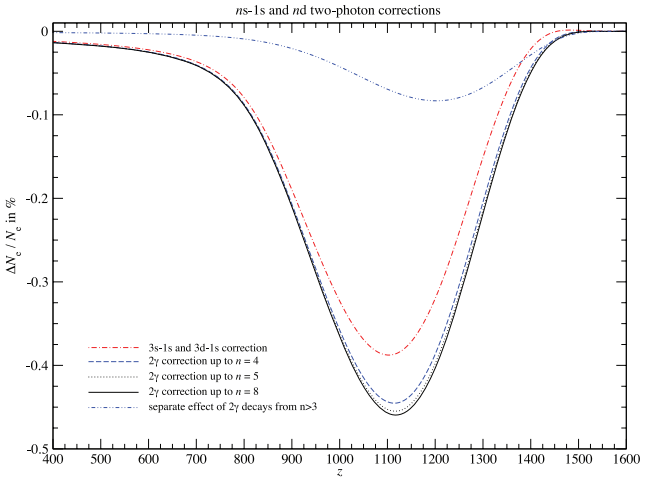

Figure 4. Two-photon corrections from highly excited levels ($n > 2$) and their convergence with n.

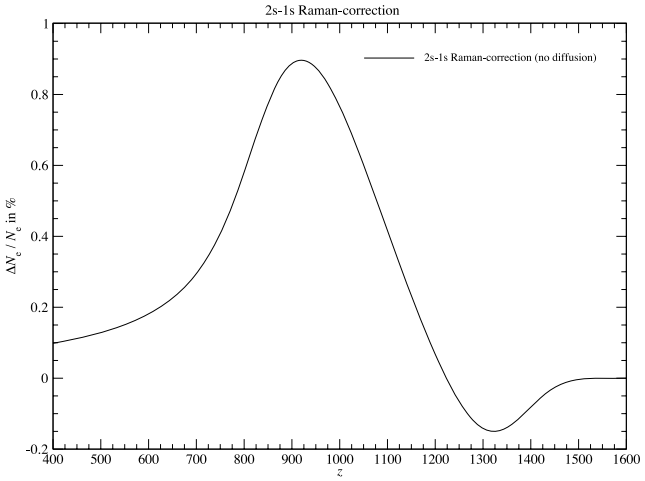

Figure 5. Raman-scattering corrections from excited levels

The main contribution comes from the 3s–1s and 3d–1s two-photon process, while the higher levels only add $\Delta N_{\rm e}/N_{\rm e} \sim -0.08$ per cent at $z \sim 1200$. The correction practically converges when accounting for the two-photon terms up to 5s–1s and 5d–1s. Also the result for the 3s–1s and 3d–1s two-photon process compares extremely well with our earlier computation (Chluba & Sunyaev 2010b). We conclude that for practical purposes it is sufficient to include the two-photon corrections for all ns and nd states up to $n \sim 4$–5.

5.4 Corrections caused by Raman processes

The final process we discuss is the effect of the Raman scattering, which was also investigated by Hirata (2008). The result of our computation is shown in Fig. 5, confirming that Raman scattering leads to a delay of recombination by $\Delta N_{\rm e}/N_{\rm e} \sim 0.9$ per cent at $z \sim 920$. This result is in very good agreement with the analysis of Hirata (2008). We found that the correction is dominated by the 2s–1s Raman process. Higher level Raman scattering leads to a small additional modification, which for practical purposes could be neglected. We recommend including the Raman corrections for the first three shells.

As mentioned above, the Raman correction has two separate contribution: one from the feedback of Lyman β photons on the

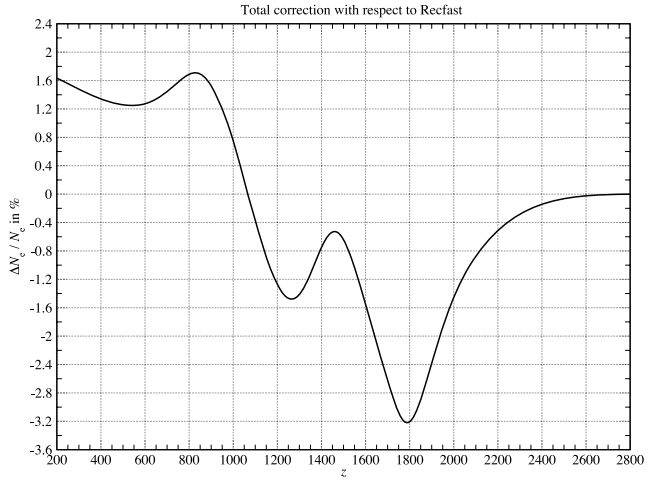

Figure 6. Total correction to the ionization history. We compared the output of our effective multilevel recombination code with RECFAST v1.4.2 (Wong & Scott 2007). However, we switched all helium flags in RECFAST off.

Lyman α resonance, which leads to a delay of recombination a low redshift, and secondly arising because of the accelerated 2s–1s scattering. The delay and acceleration need to be out of phase in redshift to create a net effect. We find that their individual contributions have amplitudes comparable to $\sim$2 per cent; however, partial cancellation makes them smaller.

5.5 Total correction with respect to RECFAST

In Fig. 6, we show the cumulative correction to the ionization history caused by all the processes included into our present recombination code. The changes during hydrogen recombination found here are very similar to those presented in Rubiño-Martín et al. (2010). The only major difference is visible at low redshifts, since their analysis was based on the results from a 100-shell hydrogen recombination model and hence the low-redshift freeze-out tail was overestimated (see Fig. 3 and comments in Chluba et al. 2010). However, as argued earlier (Fendt et al. 2009; Chluba et al. 2010; Rubiño-Martín et al. 2010), we expect that this additional modification does not affect the conclusions of their work at a significant level. In particular, they showed that the cumulative effect of all published recombination corrections could lead to biases in the values of $\Omega_b h^2$ and n_S which reach $\sim -1.7\sigma$ and $\sim -2.3\sigma$, respectively. For the analysis of CMB data from the *PLANCK Surveyor*, these corrections have to be taken into account carefully when answering queries about different models of *inflation*.

6 CONCLUSIONS

In this paper, we complete our analysis on the importance of the two-photon transitions and Raman scattering during the cosmological recombination epoch. We explicitly solve the radiative transfer equation for the H I Lyman-series transport, including all important processes (e.g. resonance scattering, full time-dependence), extending our former treatment to account for the Raman scattering as well as two-photon transition from highly excited levels with $n > 3$. Our computations are performed using an effective multilevel approach for hydrogen to accelerate the recombination calculation, which without optimization achieves run times of $\sim$1–2 min.

We find that 2s–1s Raman scattering leads to a small initial acceleration of recombination at high redshifts, which then turns into a deceleration of $\Delta N_e/N_e \sim 0.9$ per cent at $z \sim 920$. ns–1s and nd–1s Raman processes from levels with $n > 2$ only result in a small additional correction. Two-photon transitions from ns and nd states with $n > 3$ accelerate hydrogen recombination by additional $\Delta N_e/N_e \sim -0.08$ per cent at $z \sim 1200$. For practical purposes, one only has to include the two-photon corrections for the first $\sim$4–5 shells.

This work carves a path towards a new cosmological recombination code, COSMOREC, that supersedes the physical model included in RECFAST and can be used in the analysis of future CMB data, e.g. from the *PLANCK Surveyor*, ACT, SPT and *CMBPOL*. The final step will perform a detailed code comparison, and to optimize the implementation of the recombination code, so that run times of seconds can be accomplished, incorporating all the important physical processes without requiring any fudge factors. Our final version of COSMOREC will be available at www.Chluba.de/CosmoRec.

ACKNOWLEDGMENTS

The authors thank the anonymous referee for comments on the manuscript, which helped improve the paper. JC wishes to thanks Chris Hirata, Yacine Ali-Haimoud and Dan Grin for useful and stimulating discussion about recombination processes. Furthermore, JC is very grateful for additional financial support from the Beatrice D. Tremaine Fellowship 2010. Also, the authors acknowledge the use of the GPC supercomputer at the SciNet HPC Consortium. SciNet is funded by the Canada Foundation for Innovation under the auspices of Compute Canada, the Government of Ontario, Ontario Research Fund – Research Excellence and the University of Toronto.

REFERENCES

Abramowitz M., Stegun I. A., 1972, Handbook of Mathematical Functions. Dover Press, New York
Ali-Haïmoud Y., Hirata C. M., 2010, Phys. Rev. D, 82, 063521
Ali-Haïmoud Y., Grin D., Hirata C. M., 2010, preprint (arXiv:1009.4697)
Antia H. M., 2002, Numerical Methods for Scientists and Engineers. Birkhäuser Verlag, Basel
Basko M. M., 1978a, Sov. Phys.: JETP, 48, 644
Basko M. M., 1978b, Zh. Eksp. Teor. Fiz., 75, 1278
Chen X., Kamionkowski M., 2004, Phys. Rev. D, 70, 043502
Chluba J., 2010, MNRAS, 402, 1195
Chluba J., Sunyaev R. A., 2006a, A&A, 458, L29
Chluba J., Sunyaev R. A., 2006b, A&A, 446, 39
Chluba J., Sunyaev R. A., 2007, A&A, 475, 109
Chluba J., Sunyaev R. A., 2008, A&A, 480, 629
Chluba J., Sunyaev R. A., 2009a, A&A, 503, 345
Chluba J., Sunyaev R. A., 2009b, A&A, 496, 619
Chluba J., Sunyaev R. A., 2010a, MNRAS, 402, 1221
Chluba J., Sunyaev R. A., 2010b, A&A, 512, A53
Chluba J., Vasil G. M., Dursi L. J., 2010, MNRAS, 407, 599
Dubrovich V. K., Grachev S. I., 2005, Astron. Lett., 31, 359
Fendt W. A., Chluba J., Rubiño-Martín J. A., Wandelt B. D., 2009, ApJS, 181, 627
Galli S., Melchiorri A., Smoot G. F., Zahn O., 2009, Phys. Rev. D, 80, 023508
Grin D., Hirata C. M., 2010, Phys. Rev. D, 81, 083005
Hirata C. M., 2008, Phys. Rev. D, 78, 023001
Hirata C. M., Switzer E. R., 2008, Phys. Rev. D, 77, 083007
Hirata C. M., Forbes J., 2009, Phys. Rev. D, 80, 023001
Hummer D. G., 1962, MNRAS, 125, 21
Jackson J. D., 1998, Classical Electrodynamics, 3rd edn. Wiley-VCH, Hoboken, NJ
Jentschura U. D., 2009, Phys. Rev. A, 79, 022510
Kaplinghat M., Scherrer R. J., Turner M. S., 1999, Phys. Rev. D, 60, 023516

Karshenboim S. G., Ivanov V. G., 2008, Astron. Lett., 34, 289
Kholupenko E. E., Ivanchik A. V., 2006, Astron. Lett., 32, 795
Komatsu E. et al., 2010, preprint (arXiv:1001.4538)
Labzowsky L. N., Shonin A. V., Solovyev D. A., 2005, J. Phys. B: Atomic Molecular Optics., 38, 265
Labzowsky L., Solovyev D., Plunien G., 2009, Phys. Rev. A, 80, 062514
Lee H.-W., 2005, MNRAS, 358, 1472
Padmanabhan N., Finkbeiner D. P., 2005, Phys. Rev. D, 72, 023508
Rubiño-Martín J. A., Chluba J., Sunyaev R. A., 2008, A&A, 485, 377
Rubiño-Martín J. A., Chluba J., Fendt W. A., Wandelt B. D., 2010, MNRAS, 403, 439
Rybicki G. B., 2006, ApJ, 647, 709
Rybicki G. B., dell'Antonio I. P., 1994, ApJ, 427, 603
Sazonov S. Y., Sunyaev R. A., 2000, ApJ, 543, 28
Scóccola C. G., Landau S. J., Vucetich H., 2009, Mem. Soc. Astron. Ital., 80, 814
Seager S., Sasselov D. D., Scott D., 1999, ApJ, 523, L1
Seager S., Sasselov D. D., Scott D., 2000, ApJS, 128, 407
Sunyaev R. A., Zeldovich Y. B., 1970, Ap&SS, 7, 3
Switzer E. R., Hirata C. M., 2008, Phys. Rev. D, 77, 083006
Wong W. Y., Scott D., 2007, MNRAS, 375, 1441
Wong W. Y., Moss A., Scott D., 2008, MNRAS, 386, 1023
Zeldovich Y. B., Sunyaev R. A., 1969, Ap&SS, 4, 301

APPENDIX A: COMPUTING THE TWO-PHOTON EMISSION AND RAMAN PROFILES

A1 Two-photon emission profiles

We compute the two-photon decay profiles according to Chluba & Sunyaev (2009b) and Chluba & Sunyaev (2010b). In their treatment, the infinite sum over intermediate np states is split up into levels with principal quantum numbers $n > n_i$ and $n \leq n_i$, where n_i is the principal quantum number of the initial state. This makes the sum over resonances (in the case of 3s and 3d only one) finite and allows to use interpolation or fitting formulae for the remaining contributions to the total matrix element from the infinite sum.

We tabulate the non-resonant parts of the two-photon matrix elements prior to the computation. The resonances are analytically added afterwards. As explained in Chluba & Sunyaev (2010b), close to the resonances, the motion of the atoms becomes important, leading to a broadening of the two-photon profiles. To include the effect of motion on the shape of the lines close to the Doppler core, we take the ratio, $\rho_i^{2\gamma} = \varphi_i^{2\gamma}/\varphi_i^{\Sigma\Lambda}$, of the vacuum two-photon profiles to the sum of Lorentzians, and tabulate it on the computational grid in frequency. For every evaluation in time, we first compute the Voigt profiles for the resonances of interest and then sum these with their respective weights to obtain the total Voigt profile of the resonance. These are then multiplied by $\rho_i^{2\gamma}$ to obtain an approximation for the two-photon profile in the lab frame.

This procedure also allows us to include the changes in the total width, $\Gamma_{n\mathrm{p}}$, of the resonances with redshift. In vacuum, this width is related to the total decay rate; however, with the CMB this rate can change at the level of $\sim$10 per cent for the Lyman-n line when $n > 2$.

A2 Raman profiles

A ns–1s and nd–1s Raman process has form $\mathrm{H}^* + \gamma \rightarrow \mathrm{H} + \gamma'$, where H^* denotes a neutral hydrogen atom in an excited ns/nd state. In contrast to the two-photon emission process, $\mathrm{H}^* \rightarrow \mathrm{H} + \gamma + \gamma'$, the Raman process only works when photons are available. In vacuum, no Raman-scattering events occur. The ns–1s and nd–1s Raman-scattering matrix elements are related to the ns–1s and nd–1s two-photon matrix elements by *crossing-symmetry*. The energies of the incoming photon, γ, and the outgoing photon, γ', are given by $\nu + \nu_{j1\mathrm{s}} = \nu'$, where $h\nu_{j1\mathrm{s}}$ is the excitation energy of the initial state with respect to the ground state.

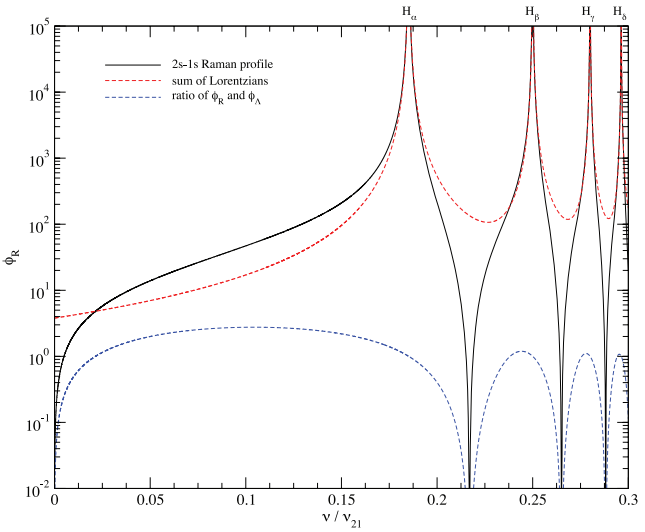

Figure A1. Frequency dependence of the 2s–1s Raman profile. This profile has to be interpreted as a scattering cross-section, where the electron is in the excited state. The positions of the Balmer α, β, γ and δ resonances are marked. For comparison, the cross-section computed as a sum of Lorentzians is shown. Furthermore, we also show the ratio of these two profiles, indicating that close to the resonances the profile becomes Lorentzian, with small corrections.

Raman-scattering profiles can be derived using the formulae given in Chluba & Sunyaev (2010b). The main differences are: (i) in the functions $f_n(y)$ and $h_n(y)$ (see equations 8c and 10d in their paper) $y = \nu/\nu_{j1\mathrm{s}}$ has to be replaced with $-y$; (ii) the pre-factor $y^3(1-y)^3$ needs to be substituted by $y^3(1+y)^3$ and (iii) the resonances now appear for intermediate np states with $n > n_j$, where n_j is the principal quantum number of the initial state.

For a given computational frequency grid, only a finite number of resonances appear, say for $n_j < n \leq n_{\mathrm{res}}$. Like in computations of the two-photon emission profiles, one can therefore split the infinite sum over intermediate p states (including the continuum) into resonant and non-resonant contributions. The non-resonant contributions come from $n < n_j$ and $n_{\mathrm{res}} < n$, where the non-resonant matrix element scales like $1/y$ for $y \rightarrow 0$ and $[1/(n_j^2 - 1) - y]^{-1}$ towards the ionization threshold, $\nu \rightarrow \nu_{j\mathrm{c}}$. One can, therefore, tabulate $M_{\mathrm{nr}}\; y\,[1/(n_j^2 - 1) - y]$ on a grid and add the finite number of remaining resonances analytically. The pole displacements arising from the finite lifetime of the intermediate p state, as mentioned in Chluba & Sunyaev (2010b), have to be included.

In Figs A1 and A2, we present some examples of Raman-scattering profiles. The electron is assumed to be in the excited state, so that a low-frequency photon can Raman scatter off the atom. In the recombination problem, these photons will be drawn from the CMB blackbody, as spectral distortions below the Balmer continuum can be neglected. Figs A1 and A2 also show the ratios of the Raman profiles with respect to the sum of Lorentzians. Close to the resonances, all these ratios are extremely close to unity as expected. We use this ratio to include the effect of motion of the atom on the shape of the resonances close to the Doppler core as explained in the previous section.

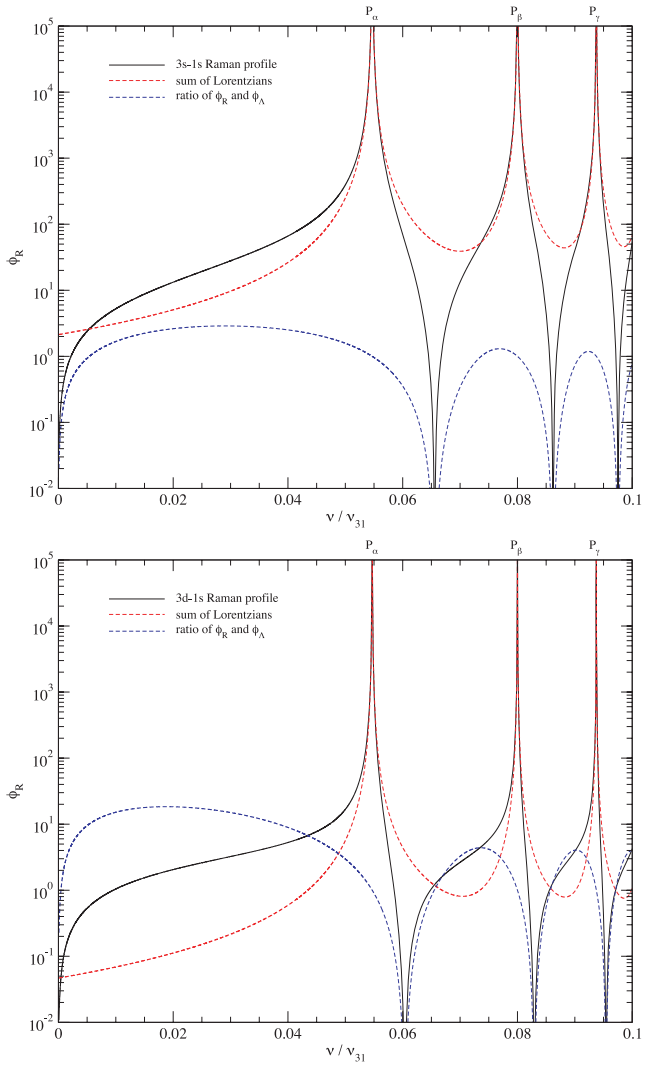

Figure A2. Same as Fig. A1, but for the 3s–1s and 3d–1s Raman profiles. We marked the positions of the Paschen α, β and γ resonances.

APPENDIX B: PARTIAL DIFFERENTIAL EQUATION SOLVER

For this work, we implement our own partial differential equation (PDE) solver in order to fine-tune performance and precision. Comparing with previous results obtained using the NAG library confirms the precision of our own implementation.

The PDE describing the radiative transfer problem during recombination is of the *parabolic* type. It is desirable to use an implicit or a semi-implicit numerical scheme to avoid strong limitation on the step size imposed by stability. Several numerical algorithms for this type of problems have been discussed, e.g. Crank–Nicolson method (see Antia 2002).

For the recombination problem, it is beneficial to use a *non-uniform* grid in frequency as in the vicinity of the resonances one needs a resolution of $\Delta\nu/\nu \sim 10^{-7}$ to 10^{-5}, while a much coarser grid can be introduced outside this zone. However, this implies that the spatial discretization that is normally used in the Crank–Nicolson method is only accurate to first order in the grid spacing. We therefore decided to implement a second-order scheme in which the first and second derivatives of the occupation number n_x with respect to frequency can be written as

$$\frac{\partial n_x}{\partial x} = \sum_i \kappa_i(x)\, n_{x_i}, \tag{B1}$$

$$\frac{\partial^2 n_x}{\partial x^2} = \sum_i \Lambda_i(x)\, n_{x_i}, \tag{B2}$$

where the sums run over five grid-points in the neighbourhood of x. The coefficients $\kappa_i(x)$ and $\Lambda_i(x)$ can be easily derived using Lagrange interpolation formulae (e.g. see Abramowitz & Stegun 1972). These coefficients can then be pre-computed and stored once the grid is chosen. The PDE appearing in the diffusion problem can thus be written as matrix equation,

$$\mathbf{B}_{ij}\, n_{x_j} = b_i, \tag{B3}$$

where the matrix, $\mathbf{B}_{ij}$, is banded[18] with four off-diagonal elements. Such system can be easily solved with $\mathcal{O}(M)$ operations, where M denotes the number of grid-points.

For each resonance, we typically needed $\sim 10^3$ points in frequency. Increasing this number to $\sim 10^4$ per resonance did not make a notable difference for the final correction to the ionization history. Our typical step size in redshift was $\Delta z \sim 1$, but we also tried a ten times smaller time-step, without finding any significant modification in the solution. Our tests also showed that even $\Delta z \sim 10$ should be sufficient for detailed computations of the ionization history.

Furthermore, we tried fully implicit and semi-implicit schemes (θ method with $\theta > 0.5$) finding good performance for $\theta \sim 0.6$. We also experimented with the distribution of grid points, and found that it is important to sample the Doppler core well.

[18] At the boundary, the matrix is not perfectly banded, but this does not pose a big problem.

This paper has been typeset from a TEX/LATEX file prepared by the author.